Biogeosciences Discuss., doi:10.5194/bg-2016-278, 2016
Manuscript under review for journal Biogeosciences
Published: 18 July 2016

Biogeosciences
Discussions
Open Access
EGU

1 **Air-water CO_2 evasion from U.S. East Coast estuaries**

2 Goossens, Nicolas[1], Laruelle, Goulven Gildas[1*], Arndt, Sandra[2], Cai, Wei-Jun[3] & Regnier, Pierre[1]

3

4 1 Department Geosciences, Environment and Society, Université Libre de Bruxelles, Brussels,
5 Belgium
6 2 School of Geographical Sciences, University of Bristol, Bristol, UK
7 3 School of Marine Science and Policy, University of Delaware, Newark, Delaware, USA
8
9 *corresponding author: goulven.gildas.laruelle@ulb.ac.be
10
11

Biogeosciences Discuss., doi:10.5194/bg-2016-278, 2016
Manuscript under review for journal Biogeosciences
Published: 18 July 2016

Abstract:

This study presents the first regional-scale assessment of estuarine CO_2 evasion along the East coast of the US (25 – 45 °N). The focus is on 43 tidal estuaries, which together drain a catchment of 697 10^3 km2 or 76 % of the total area within this latitudinal band. The approach is based on the Carbon – Generic Estuarine Model (C-GEM) that allows simulating hydrodynamics, transport and biogeochemistry for a wide range of estuarine systems using readily available geometric parameters and global databases of seasonal climatic, hydraulic, and riverine biogeochemical information. Together, US East coast estuaries emit 1.9 TgC yr^{-1}, which correspond to about 40 % of the carbon inputs from rivers, marshes and mangroves. Carbon removal within estuaries results from a combination of physical (outgassing of supersaturated riverine waters) and biogeochemical processes (net heterotrophy and nitrification). The CO_2 evasion and its underlying drivers show important variations across individual systems, but reveal a clear latitudinal pattern characterized by a decrease in the relative importance of physical over biogeochemical processes along a North-South gradient. Finally, results reveal that the ratio of estuarine surface area to the river discharge, S/Q (which has a scale of per meter discharged water per year), could be used as a predictor of the estuarine carbon processing in future regional and global scale assessments.

Biogeosciences Discuss., doi:10.5194/bg-2016-278, 2016
Manuscript under review for journal Biogeosciences
Published: 18 July 2016

1 Introduction

Carbon fluxes along the land-ocean aquatic continuum are currently receiving increasing attention because of their recently recognized role in the global carbon cycle and anthropogenic CO_2 budget (Bauer et al., 2013; Regnier et al., 2013a; LeQuéré et al., 2014, 2015). Estuaries are important reactive conduits along this continuum, which links the terrestrial and marine global carbon cycles (Cai, 2011). Large amounts of terrestrial carbon transit through these systems, where they mix with carbon from autochthonous, as well as marine sources. During estuarine transit, heterotrophic processes degrade a fraction of the allochthonous and autochthonous organic carbon inputs, supporting a potentially significant, yet poorly quantified CO_2 evasion flux to the atmosphere. Recent estimates suggest that 0.15-0.25 PgC yr^{-1} is emitted from estuarine systems worldwide (Borges and Abril, 2012; Cai, 2011; Laruelle et al., 2010; Regnier et al., 2013a; Laruelle et al., 2013, Bauer et al., 2013). Thus, in absolute terms the global estuarine CO_2 evasion corresponds to about 15% of the open ocean CO_2 uptake despite the much smaller total surface area.

Currently, estimates of global estuarine CO_2 emissions are mainly derived on the basis of data-driven approaches that rely on the extrapolation of local measurements (Cai, 2011; Chen et al., 2013; Laruelle et al., 2013). While these approaches provide useful first-order estimates, they fail to capture the spatial and temporal heterogeneity of the estuarine environment (Bauer et al., 2013). In addition, these global estimates are biased towards anthropogenically influenced estuarine systems located in industrialized countries (Regnier et al., 2013a). Furthermore, observation-based approaches do not provide insights into the complex and dynamic interplay of biogeochemical and physical processes that controls estuarine CO_2 fluxes. In this respect, integrated model-data approaches provide a suitable alternative. Reaction transport models (RTMs) allow, in conjunction with data, the investigation of the estuarine response over the entire spectrum of fluctuating forcing conditions, including the long-term effect of land-use and climate changes (Bauer et al., 2013; Paerl et al., 2006; Thieu et al., 2010). In addition, RTMs can fully resolve the dynamic interplay of transport and transformation processes that control CO_2 fluxes across the entire estuarine gradient and at a

Biogeosciences Discuss., doi:10.5194/bg-2016-278, 2016
Manuscript under review for journal Biogeosciences
Published: 18 July 2016

high temporal and spatial resolution (Arndt et al., 2009; Arndt et al., 2011; Vanderborght et al., 2002; Volta et al., 2014). Integrated model-data approaches thus have the potential to significantly advance our mechanistic and quantitative understanding of global estuarine CO_2 fluxes, as well as their response to global change. RTMs have recently been successfully applied to quantify system-wide, integrated biogeochemical indicators, such as Net Ecosystem Metabolism (Volta et al., 2014), carbon and nutrients budgets (Soetaert and Herman, 1995; Vanderborght et al., 2002; Billen et al., 2009; Laruelle et al., 2009) or nutrient filtering capacities (Arndt et al., 2009). To our knowledge, however, published modeling studies dedicated to quantifying estuarine CO_2 dynamics remain limited to the Scheldt estuary in Belgium-The Netherlands (Hofmann et al., 2008; Vanderborght et al., 2002) and to the Elbe in Germany (Volta et al., 2016a). Recently, Regnier et al., (2013b) quantified the contribution of different biogeochemical processes for CO_2 air-water fluxes in an idealized, funnel-shaped estuary forced by typical summer conditions characterizing a temperate Western European climate. Volta et al. (2016b) further investigated the effect of estuarine geometry on the CO_2 outgassing using three idealized systems. Using a similar approach, Volta et al. (2016a) established the first regional carbon budget for estuaries surrounding the North Sea by explicitly simulating the six largest systems of the area. Yet, local and regional quantifications of estuarine CO_2 fluxes using such an integrated data-RTM approach remain extremely limited and a RTM-based global quantification of estuarine CO_2 fluxes is currently lacking.

The lack of regional or global evaluations of the estuarine carbon dynamics can be partly explained by the high computational costs of RTM simulations. In addition, significant data requirements, such as comprehensive bathymetric and geometric information and boundary conditions may further limit the applicability of RTMs on a regional or global scale, while the need for benchmarking on a number of extensively surveyed, representative systems provides additional constraints. In attempt to overcome these constraints, the Carbon-Generic Estuary Model (C-GEM; Volta et al., 2014) has been developed with the aim of enabling the quantification of biogeochemical dynamics in estuaries on a regional and global scale. The focus is on tidal systems as defined by Dürr et al. (2011) and the

Biogeosciences Discuss., doi:10.5194/bg-2016-278, 2016
Manuscript under review for journal Biogeosciences
Published: 18 July 2016

approach is based on a one-dimensional, time-dependent representation of hydrodynamic, transport and reaction processes within an estuary. C-GEM is computationally efficient and reduces data requirements by using an idealized representation of the geometry to support the hydrodynamic calculations and, subsequently, transport and biogeochemical reaction processes. The C-GEM modeling platform thus enables hundreds to thousands of steady state or fully transient simulations spanning years to decades for a multitude of estuarine systems, using geometric information readily available through maps or remote sensing images. Despite the geometric simplification, C-GEM resolves the most important temporal and spatial scales characterizing the estuarine dynamics and provides an accurate description of the hydrodynamics, transport and biogeochemistry in tidal estuaries (Volta et al., 2014).

Here, an extended version of C-GEM (v1.0) is applied to quantify CO_2 exchange fluxes, as well as the overall organic and inorganic carbon budgets for the full suite of estuarine systems located along the entire East coast of the United States. The applied RTM approach allows to evaluate the relative significance of different physical and biogeochemical processes for the regional-scale CO_2 evasion within the ensemble of estuarine filters along the selected coastal segment, which is one of the most intensively monitored regions in the world. A unique set of regional data, including river and continental shelf sea partial pressure of CO_2 (pCO_2; Signorini et al., 2013; Laruelle et al., 2015), riverine biogeochemical properties (Lauerwald et al., 2013), estuarine eutrophication status (Bricker et al., 2007) and estuarine morphology (NOAA, 1985) are available. These comprehensive data sets are complemented by local observations of carbon cycling and CO_2 fluxes in selected, individual estuarine systems (see Laruelle et al., 2013 for a review), making the East coast of the United States an ideal region for a first, fully explicit regional evaluation of CO_2 evasion resolving every major tidal estuary along the selected coastal segment. The scale addressed in the present study is unprecedented so far (> 3000 km of coastline) and covers a wide range of estuarine morphological features, climatic conditions, land-use and land cover types, as well as urbanization levels.

Biogeosciences Discuss., doi:10.5194/bg-2016-278, 2016
Manuscript under review for journal Biogeosciences
Published: 18 July 2016

2. Regional description and model approach

2.1 Observation-based carbon budget for the East coast of the United States

The study area covers the Atlantic coast of the United States (Fig.1), from the southern tip of Florida (25°N) to Cobscook Bay (45°N) at the US-Canada boundary. This area encompasses distinct climatic zones and land cover types and exhibits a variety of morphologic features (Figure 1). The region can be subdivided into several sub-regions following a latitudinal gradient (Signorini et al., 2013). In this study, we define three sub-regions following the boundaries suggested by the COSCAT segmentation (Meybeck et al., 2006; Laruelle et al., 2013) and the further subdivision described in Laruelle et al. (2015). From North to South, the regions are called North Atlantic, Mid Atlantic and South Atlantic Regions (Figure 1). Total carbon inputs from watersheds to US East coast estuaries (Table 1) have been estimated to range from 4.0 to 10.7 Tg C yr^{-1} (Mayorga et al., 2010; Shih et al., 2010; Stets and Strieg, 2012; Tian et al., 2010; Tian et al., 2012), consisting of dissolved organic carbon (DOC; ~50%), dissolved inorganic carbon (DIC; ~40%) and particulate organic carbon (POC; ~10%). In addition, a statistical approach has been applied to estuaries of the region to quantify organic carbon budgets and Net Ecosystem Productivity (NEP) using empirical models (Herrmann et al., 2015).

Recent studies estimated that, along the East coast of the United States, rivers emit 11.4 TgC yr^{-1} of CO_2 to the atmosphere (Raymond et al., 2013), while continental shelf waters absorb between 3.4 and 5.4 TgC yr^{-1} of CO_2 from the atmosphere (Signorini et al., 2013). A total of thirteen local, annual mean estuarine CO_2 flux estimates across the air-water interface based on measurements are also reported in the literature and are grouped along a latitudinal gradient (fig 1). Four of these estimates are located in the South Atlantic region (SAR): Sapelo Sound, Doboy Sound, Altamaha Sound (Jiang et al., 2008), and the Satilla River estuary (Cai and Wang, 1998). Three studies investigate CO_2 fluxes in the mid-Atlantic Region (MAR): the York River Estuary (Raymond et al., 2000) and the Hudson River (Raymond et al., 1997). There is also a comprehensive CO_2 flux study for the Delaware Estuary published after the completion of this work (Joeseof et al., 2015). Six systems are located in the

Biogeosciences Discuss., doi:10.5194/bg-2016-278, 2016
Manuscript under review for journal Biogeosciences
Published: 18 July 2016

North Atlantic region (NAR): The Great Bay, the Little Bay, the Oyster estuary, the Bellamy estuary, the Cocheco estuary (Hunt et al., 2010; 2011), and the Parker River estuary (Raymond and Hopkinson, 2003). The mean annual flux per unit area from these local studies is 11.7±13.1 mol C m^{-2} yr^{-1} and its extrapolation to the total estuarine surface leads to a regional CO_2 evasion estimate of 3.8 Tg C y^{-1}. This estimate is in line with that of Laruelle et al. (2013) for the same region which proposes an average CO_2 emission rate of 10.8 mol C m^{-2} yr^{-1}. Thus, CO_2 outgassing could remove 35% to 95% of the riverine carbon loads during estuarine transit. About 75 % of the air-water exchange occurs in tidal estuaries (2.8 Tg C y^{-1}) while lagoons and small deltas contribute to the remaining 25 %. Although these simple extrapolations from limited observational data are associated with large uncertainties, they highlight the potentially significant contribution of estuaries to the CO_2 outgassing in the region. However, process-based quantifications of regional organic and inorganic C budgets including air-water CO_2 fluxes for the estuarine systems along the East coast are not available.

2.2 Selection of estuaries

The National Estuarine Eutrophication Assessment (NEAA) survey (Bricker et al., 2007), which uses geospatial data from the National Oceanic and Atmospheric Administration (NOAA) Coastal Assessment Framework (CAF) (NOAA, 1985), was used to identify and characterize 64 estuarine systems discharging along the Atlantic coast of the United States. From this set, 47 'tidal' estuaries, defined as a river stretch of water that is tidally influenced (Dürr et al., 2011), were retained (fig.1) to be simulated by the C-GEM model, which is designed to represent such systems. The 15 non-tidal estuaries that are excluded from the present study are located in the SAR (10) and in the MAR (5) and account for less than 15% of the total riverine carbon loads of the region.

The northeastern part of the domain (NAR, Fig. 1; table 1) includes 20 estuaries along the Gulf of Maine and the Scotian shelf, covering a cumulative surface area of ~5300 km². It includes drowned valleys, rocky shores and a few tidal marshes. The climate is relatively cold (annual mean= 8°C) and

Biogeosciences Discuss., doi:10.5194/bg-2016-278, 2016
Manuscript under review for journal Biogeosciences
Published: 18 July 2016

155 the human influence is relatively limited because of low population density and low freshwater
156 inputs. The mean estuarine water depth is 12.9 m and the mean tidal range is 2.8 m.

157 The central zone (MAR) includes 17 tidal estuaries accounting for a total surface area of 14500 km².
158 The Chesapeake Bay and the Delaware estuaries alone contribute more than 60% to the surface area
159 of the region. In this region, estuaries are drowned valleys with comparatively high river discharge
160 and intense exchange with the ocean. Several coastal lagoons, characterized by a limited exchange
161 with the ocean are located here, but are not included in our analysis. The Mid-Atlantic Region (MAR)
162 is characterized by a mean annual temperature of 13°C and is strongly impacted by human activities,
163 due to the presence of several large cities (e.g. New York, Washington, Philadelphia, Baltimore) and
164 intense agriculture. The mean water depth is about 4.7 m and the tidal range is 0.8 m.

165 The southern Atlantic region (SAR) includes 10 tidal estuaries covering a total surface area of 12182
166 km². These systems are generally dendritic and surrounded by extensive salt marshes. The climate is
167 subtropical with an average annual temperature of 19°C. Land use includes agriculture and industry,
168 but the population density is generally low. Estuarine systems in the SAR are characterized by a
169 shallow mean water depth of 2.9m and a tidal range of 1.2 m.

170 **2.3 Model set-up**

171 The generic 1D Reactive-Transport Model (RTM) C-GEM (Volta et al., 2014) is used to quantify the
172 estuarine carbon cycling in the 47 systems considered in this study. The approach is based on
173 idealized geometries (Savenije, 2005; Volta et al., 2014) and is designed for regional and global scale
174 applications (Regnier et al., 2013b; Volta et al., 2014, 2016a). The model approach builds on the
175 premise that hydrodynamics exerts a first-order control on estuarine biogeochemistry (Arndt et al.,
176 2007; Friedrichs and Hofmann, 2001) and CO_2 fluxes (Regnier et al., 2013a). The method takes
177 advantage of the mutual dependence between geometry and hydrodynamics in tidal estuaries

Biogeosciences Discuss., doi:10.5194/bg-2016-278, 2016
Manuscript under review for journal Biogeosciences
Published: 18 July 2016

178 (Savenije, 1992) and the fact that, as a consequence, transport and mixing can be easily quantified
179 from readily available geometric data (Regnier et al., 2013a; Savenije, 2005; Volta et al., 2016b).

180 **2.3.1 Description of idealized geometries for tidally-averaged conditions**

181 Although tidal estuaries display a wide variety of shapes, they nevertheless share common
182 geometric characteristics that are compatible with an idealized representation (Fig 2, Savenije, 1986;
183 Savenije, 2005). For tidally-averaged conditions, their width B (or cross-sectional area A) can be
184 described by an exponential decrease as a function of distance, *x*, from the mouth (Savenije, 1986;
185 Savenije, 2005):

$$B = B0 * \exp\left(-\frac{x}{b}\right) \quad (1)$$

186 where B (m) is the tidally averaged width, B0 (m) the width at the mouth, x (m) the distance from
187 the mouth (x=0) and b (m) the width convergence length (Fig. 2). The width convergence length, b, is
188 defined as the distance between the mouth and the point at which the width is reduced to B0 e^{-1}. It
189 is directly related to the dominant hydrodynamic forcing. A high river discharge typically results in a
190 prismatic channel with long convergence length (river dominated estuary), while a large tidal range
191 results in a funnel-shaped estuary with short convergence length (marine dominated estuary). At the
192 upstream boundary, the estuarine width is given by:

$$B_L = B0 * \exp\left(-\frac{L}{b}\right) \quad (2)$$

193 Where L denotes the total estuarine length (m) along the estuarine longitudinal axis.

194 The total estuarine surface S (m^2) can be estimated by integrating equation (1) over the estuarine
195 length:

$$S = \int_0^L B\, dx = b * B0 * \left(1 - \exp\left(-\frac{L}{b}\right)\right) \quad (3)$$

196

Biogeosciences Discuss., doi:10.5194/bg-2016-278, 2016
Manuscript under review for journal Biogeosciences
Published: 18 July 2016

197 The width convergence length is then calculated from B0, B_L, L and the real estuarine surface area
198 (SR) by inserting equation (2) in equation (3):

$$b = \frac{SR}{B0 - BL} \quad (4)$$

199 SR is calculated for each system using the SRTM water body data (fig. 3a), a geographical dataset
200 encoding high-resolution worldwide coastal outlines in a vector format (NASA/NGA, 2003). While
201 such a database exists for a well monitored region such as the East coast of the US, resorting to
202 using the idealized estuarine surface area (S) is necessary in many other regions. The longitudinal
203 mean, tidally averaged, depth h (m), is obtained from the National Estuarine Eutrophication
204 Assessment database (Bricker et al., 2007).

205 Using this idealized representation, the estuarine geometry can be defined by a limited number of
206 parameters: the width at the mouth (B_0), the estuarine length (L), the estuarine width at the
207 upstream limit (B_L) and the mean depth h. These parameters can be easily determined through GIS,
208 local maps, Google Earth or obtained from databases (NASA/NGA, 2003).

209 **2.3.2 Hydrodynamics, transport and biogeochemistry**

210 Estuarine hydrodynamics is described by the one-dimensional barotropic, cross-sectionally
211 integrated mass and momentum conservation equations for a channel with arbitrary geometry
212 (Nihoul and Ronday, 1976; Regnier et al., 1998; Regnier and Steefel, 1999):

213 $$r_s \frac{\partial A}{\partial t} + \frac{\partial Q}{\partial x} = 0 \quad (5)$$

214 $$\frac{\partial U}{\partial t} + U\frac{\partial U}{\partial x} = -g\frac{\partial \zeta}{\partial x} - g\frac{U|U|}{C^2 H} \quad (6)$$

215 where:

216 *t* time [s]

Biogeosciences Discuss., doi:10.5194/bg-2016-278, 2016
Manuscript under review for journal Biogeosciences
Published: 18 July 2016

217	x	distance along the longitudinal axis	[m]
218	A	cross-section area $A = H \cdot B$	[m^2]
219	Q	cross-sectional discharge $Q = A \cdot U$	[$m^3\ s^{-1}$]
220	U	flow velocity Q / A	[$m\ s^{-1}$]
221	r_s	storage ratio $r_s = B_s / B$	[-]
222	B_s	storage width	[m]
223	g	gravitational acceleration	[$m\ s^{-2}$]
224	ξ	elevation	[m]
225	H	total water depth $H = h + \xi(x,t)$	[m]
226	C	Chézy coefficient	[$m^{1/2}\ s^{-1}$]

227 The coupled partial differential equations (Eqs. (6) and (7)) are solved by specifying the elevation
228 $\xi_0(t)$ at the estuarine mouth and the river discharge $Q_r(t)$ at the upstream limit of the model domain.

229 The one-dimensional, tidally-resolved, advection-dispersion equation for a constituent of
230 concentration $C(x,t)$ in an estuary can be written as (e.g. Pritchard, 1958):

231 $$\frac{\partial C}{\partial t} + \frac{Q}{A}\frac{\partial C}{\partial x} = \frac{1}{A}\frac{\partial}{\partial x}\left(AD\frac{\partial C}{\partial x}\right) + P \qquad (7)$$

232 where $Q(x,t)$ and $A(x,t)$ denote the cross-sectional discharge and area, respectively and are provided
233 by the hydrodynamic model (eq. 6 and 7). $P(x,t)$ is the sum of all production and consumption
234 process rates affection the concentration of the constituent. The effective dispersion coefficient D
235 ($m^2\ s^{-1}$) implicitly accounts for dispersion mechanisms associated to sub-grid scale processes (Fischer,
236 1976; Regnier et al., 1998). In general, D is maximal near the sea, decreases upstream and becomes

Biogeosciences Discuss., doi:10.5194/bg-2016-278, 2016
Manuscript under review for journal Biogeosciences
Published: 18 July 2016

237 virtually zero near the tail of the salt intrusion curve (Preddy, 1954; Kent, 1958; Ippen and Harleman,
238 1961; Stigter and Siemons, 1967). The effective dispersion at the estuarine mouth can be quantified
239 by the following relation (Van der Burgh, 1972):

240 $$D_0 = 26 \cdot (h_0)^{1.5} \cdot (N \cdot g)^{0.5} \quad (8)$$

241 where h_0 (m) is the tidally-averaged water depth at the estuarine mouth and N is the dimensionless
242 Canter Cremers' estuary number defined as the ratio of the freshwater entering the estuary during a
243 tidal cycle to the volume of salt water entering the estuary over a tidal cycle. For each estuary, N can
244 thus be calculated directly from the hydrodynamic model. The variation in D along the estuarine
245 gradient can be described by Van der Burgh's equation (Savenije, 1986):

246 $$\frac{\partial D}{\partial x} = -K \frac{Q_r}{A} \quad (9)$$

247 where K is the dimensionless Van der Burgh's coefficient and the minus sign indicates that D
248 increases in downstream direction (Savenije, 2012). The Van der Burgh's coefficient is a shape factor
249 that has values between 0 and 1 (Savenije, 2012), and is a function of estuarine geometry for tidally
250 average conditions. Therefore, each estuarine system has its own characteristic K value, which
251 correlates with geometric and hydraulic scales (Savenije, 2005). Based on a regression analysis
252 covering a set of 15 estuaries, it has been proposed to constrain K from the estuarine geometry
253 (Savenije, 1992):

254 $$K = 4.32 \cdot \frac{h_0^{0.36}}{B_0^{0.21} \cdot b^{0.14}} \quad \text{with} \quad 0 < K < 1 \quad (10)$$

255 Reaction processes P considered in C-GEM comprise aerobic degradation, denitrification,
256 nitrification, primary production, phytoplankton mortality and air-water gas exchange for O_2 and CO_2
257 (Fig.4 and Table 2). These processes and their mathematical formulation are described in detail in
258 Volta et al. (2014) and Volta et al. (2016a).

Biogeosciences Discuss., doi:10.5194/bg-2016-278, 2016
Manuscript under review for journal Biogeosciences
Published: 18 July 2016

259 The non-linear partial differential equations for the hydrodynamics are solved by a finite difference
260 scheme following the approach of (Regnier et al., 1997), (Regnier and Steefel, 1999) and
261 (Vanderborght et al., 2002). The timestep Δt is 150s and the grid size Δx is constant along the
262 longitudinal axis of the estuary. The grid size default value is 2000m, but can be smaller for short
263 length estuaries to guarantee a minimum of 20 grid points within the computational domain.
264 Transport and reaction terms are solved in sequence within a single timestep using an operator
265 splitting approach (Regnier et al., 1997). The advection term in the transport equation is integrated
266 using a third-order accurate total variation diminishing (TVD) algorithm with flux limiters (Regnier et
267 al., 1998), ensuring monotonicity (Leonard, 1984), while a semi-implicit Crank-Nicholson algorithm is
268 used for the dispersion term (Press et al., 1992). These schemes have been extensively tested using
269 the CONTRASTE estuarine model (e.g. Regnier et al., 1998; Regnier and Steefel, 1999; Vanderborght
270 et al., 2002) and guarantee mass conservation to within <1%. The reaction network (including
271 erosion-deposition terms when the constituent is a solid species), is numerically integrated using the
272 Euler method (Press et al., 1992). The primary production dynamics, which requires vertical
273 resolution of the photic depth, is calculated according to the method described in Vanderborght et
274 al. (2007).

275 **2.4 Boundary and forcing conditions**

276 Boundary and forcing conditions are extracted from global databases and global model outputs that
277 are available at 0.5° resolution. Therefore, C-GEM simulations are performed at the same resolution
278 according to the following procedure. First, 47 coastal cells corresponding to tidal estuaries are
279 identified in the studied area (fig.1). If the mouth of an estuary is spread over several 0.5° grid cells,
280 those cells are regrouped in order to represent a single estuary (e.g. Delaware estuary), and
281 subsequently, a single idealized geometry is defined as described above.

Biogeosciences Discuss., doi:10.5194/bg-2016-278, 2016
Manuscript under review for journal Biogeosciences
Published: 18 July 2016

For each resulting cell, boundary and forcing conditions are calculated for the following periods: January-March; April-June; July-September and October-December. This allows for an explicit representation of the seasonal variability in the simulations.

2.4.1 External forcings

Transient physical forcings are calculated for each season and grid cell using monthly mean values of water temperature (World Ocean Atlas, 2009) and seasonal averaged values for wind speed (Cross-Calibrated-Multi-Platform (CCMP) Ocean Surface Wind Vector Analyses project (Atlas et al., 2011)). Mean daily solar radiation and photoperiods (corrected for cloud coverage) are calculated depending on latitude and day of the year using a simple model (Brock, 1981).

2.4.2 Riverine discharge, concentrations and fluxes

River discharges are extracted from the UNH/GRDC runoff dataset (Fekete et al., 2002). These discharges represent long-term averages (1960-1990) of monthly and annual runoff at 0.5 degree resolution. The dataset is a composite of long-term gauging data, which provides average runoff for the largest river basins, and a climate driven water balance model (Fekete et al., 2002). Total runoff values are then aggregated for each watershed at the coarser 0.5 degree resolution (fig. 3b). Next, seasonal mean values (in $m^3\ s^{-1}$) are derived in order to account for the intra-annual variability in water fluxes. Based on annual carbon and nutrients inputs from the watersheds (Mg y^{-1}), mean annual concentrations (mmol m^{-3}) are estimated for each watershed using the UNH/GRDC annual runoff ($km^3\ y^{-1}$). Mean seasonal concentrations are then calculated from the seasonally resolved river water fluxes of a given sub-region.

Annual inputs of dissolved organic carbon (DOC), particulate organic carbon (POC) and inorganic nutrients are derived from the globalNEWS2 model (Mayorga et al., 2010). Global NEWS is a spatially explicit, multi-element (N, P, Si, C) and multi-form global model of nutrient exports by rivers. In a nutshell, DOC exports are a function of runoff, wetland area, and consumptive water use (Harrison

Biogeosciences Discuss., doi:10.5194/bg-2016-278, 2016
Manuscript under review for journal Biogeosciences
Published: 18 July 2016

et al., 2005). No distinction is made between agricultural and natural landscapes, since they appear to have similar DOC export coefficients (Harrison et al., 2005). Sewage inputs of OC are ignored in GlobalNEWS, because their inclusion did not improve model fit to data (Harrison et al., 2005). POC exports from watersheds are estimated using an empirical relationship with Suspended Particulate Matter (SPM; Ludwig et al., 1996). Inorganic nitrogen (DIN) and phosphorus (DIP) fluxes calculated by GlobalNEWS depend on agriculture and tropical forest coverage, fertilizer application, animal grazing, sewage input, atmospheric N deposition and biological N fixation (Mayorga et al., 2010). The inputs of dissolved silica (DSi) are controlled by soil bulk density, precipitation, slope, and presence of volcanic lithology (Beusen et al., 2009).

The DIN speciation is not provided by the GlobalNEWS2 model. The NH_4 and NO_3 concentrations are therefore determined independently on the basis of an empirical relationship between ammonium fraction (NH4/DIN ratio) and DIN loads (Meybeck, 1982). Dissolved Oxygen (DO) concentrations are extracted from the water quality criteria recommendations published by the United States Environmental Protection Agency (EPA, 2009). The same source is used for phytoplankton concentrations, using a chlorophyll-a to phytoplankton carbon ratio of 50 gC $gChla^{-1}$ (Riemann et al., 1989) to convert the EPA values to carbon units used in the present study.

Inputs of dissolved inorganic carbon (DIC) and total Alkalinity (ALK) are calculated from values reported in the GLORICH database (Hartmann et al., 2009). For each watershed, seasonal mean values of DIC and ALK concentrations are estimated from measurements performed at the sampling locations that are closest to the river-estuary boundary. The spatial distribution of annual inputs of TOC=DOC+POC, DIC, and TC=TOC+DIC from continental watersheds to estuaries are reported in Fig.5a, 5c and 5d, respectively. The contribution of tidal wetlands to the TOC inputs is also shown (fig 5b). Overall, the TC input over the entire model domain is estimated at 4.6 Tg C yr^{-1}, which falls in the lower end of previous reported estimations (Najjar et al. 2012).

Biogeosciences Discuss., doi:10.5194/bg-2016-278, 2016
Manuscript under review for journal Biogeosciences
Published: 18 July 2016

331 **2.4.3 Inputs from tidal wetlands**

332 The DOC input of estuarine wetlands (Fig. 5b) scales to their surface area W and is calculated using
333 the GlobalNEWS parameterization:

$$Y\_DOC = \frac{\left[(E\_C_{wet} * W) + E\_C_{dry} * (1 - W)\right] * R^{a} * Q_{act}}{Q_{nat}} \quad (11)$$

334

$$\frac{Y\_DOC_{wet}}{Y\_DOC} = \frac{E\_C_{wet} * W}{E\_C_{wet} * W + E\_C_{dry} * (1 - W)} \quad (12)$$

335

336 where Y_DOC is the DOC yield (kg C km^{-2} y^{-1}) calculated for the entire watershed, Y_DOC_{wet} is the
337 estimated DOC yield from wetland areas (kg C km^{-2} y^{-1}), Q_{act}/Q_{nat} is the ratio between the measured
338 discharge after dam construction and before dam construction, E_C_{wet} and E_C_{dry} (kg C km^{-2} y^{-1}) are
339 the export coefficients of DOC from wetland and non-wetland soils, respectively. W is the
340 percentage of the land area within a watershed that is covered by wetlands, R is the runoff (m y^{-1})
341 and a is a unit-less coefficient defining how non-point source DOC export responds to runoff. The
342 carbon load Y_DOC_{wet} is then exported as a diffuse source along the relevant portions of estuary. The
343 estuarine segments receiving carbon inputs from tidal wetlands are identified using the National
344 Wetlands Inventory of the U.S. Fish and Wildlife Service (U.S. Fish and Wildlife Service, 2014). The
345 inputs from those systems are then allocated to the appropriate grid cell of the model domain using
346 GIS. The flux calculated is an annual average that is subsequently partitioned between the four
347 seasons as a function of the mean seasonal temperature, assumed to be the main control of the
348 wetland-estuarine exchange. This procedure reflects the observation that in spring and early
349 summer, DOC export is small as a result of its accumulation in the salt marshes induced by the high
350 productivity (Dai and Wiegert, 1996), (Jiang et al., 2008). In late summer and fall, the higher water
351 temperature and greater availability of labile DOC contribute to higher bacterial remineralization

Biogeosciences Discuss., doi:10.5194/bg-2016-278, 2016
Manuscript under review for journal Biogeosciences
Published: 18 July 2016

rates in the intertidal marshes (Cai et al., 1999; Middelburg et al., 1996; Wang and Cai, 2004), which induce an important export. This marsh production-recycle-export pattern is consistent with the observed excess DIC signal in the offshore water (Jiang et al. 2013). DIC export from tidal wetlands is neglected here because it is assumed that OC is not degraded before reaching the estuarine realm. Although this assumption may lead to an overestimation of OC export from marshes and respiration in estuarine water, it will not significantly affect the water pCO_2 and degassing in the estuarine waters because mixing is faster than respiration.

2.4.4 Concentrations at the estuarine mouth

For each estuary, the downstream boundary is located 20 km beyond the mouth to minimize the bias introduced by the choice of a fixed concentration boundary condition to characterize the ocean water masses (e.g. Regnier et al., 1998). This approach also reduces the influence of marine boundary conditions on the simulated estuarine dynamics, especially for all organic carbon species whose concentrations are fixed at zero at the marine boundary. DIC concentrations are extracted from the GLODAP dataset (Key et al., 2004), from which ALK and pH are calculated assuming CO_2 equilibrium between coastal waters and the atmosphere. The equilibrium value is computed using temperature (WOA2009, Locarnini et al., 2010) and salinity (WOA2009, Antonov et al. (2010)) data which vary both spatially and temporally. The equilibrium approach is a reasonable assumption because differences in partial pressure ΔpCO_2 between coastal waters and the atmosphere are generally much smaller (0-250 µatm (Signorini et al., 2013)) than those reported for estuaries (ΔpCO_2 in the range 0-10000 µatm (Borges and Abril, 2012)). Salinity, DO, NO_3, DIP and DSi concentrations are derived from the World Ocean Atlas (Antonov et al., 2010; Garcia et al., 2010a; Garcia et al., 2010b). NH_4 concentrations are set to zero in marine waters. For all variables, seasonal means are calculated for each grid cell of the domain.

Biogeosciences Discuss., doi:10.5194/bg-2016-278, 2016
Manuscript under review for journal Biogeosciences
Published: 18 July 2016

376 **2.5 Biogeochemical indicators**

377 The model outputs (longitudinal profiles of concentration and reaction rates) are integrated in time
378 over the entire volume or surface of each estuary to produce the following indicators of the
379 estuarine biogeochemical functioning (Regnier et al., 2013b): the mean annual Net Ecosystem
380 Metabolism (*NEM*), the air-water CO_2 flux (FCO_2), the carbon and nitrogen filtering capacity (*CFilt*
381 and *NFilt*) and their corresponding element budgets. The *NEM* (molC y^{-1}) (Caffrey, 2004; Odum,
382 1956) is defined as the difference between net primary production (*NPP*) and total heterotrophic
383 respiration (*HR*) at the system scale:

$$NEM = \int_0^{365} \int_0^{L} [NPP(x,t) - R_{aer}(x,t) - R_{den}(x,t)] * B(x) * H(x,t)\, dx\, dt \quad (13)$$

384

385 where *NPP* is the Net Primary Production (mol C m^{-3} y^{-1}), R_{aer} the aerobic degradation of organic
386 matter (in mol C m^{-3} y^{-1}) and R_{den} the denitrification (in mol C m^{-3} y^{-1}) (see Volta et al., 2014 for
387 detailed formulations). *NEM* is thus controlled by the production and decomposition of
388 autochthonous organic matter, by the amount and degradability of organic carbon delivered by
389 rivers and tidal wetlands and by the export of terrestrial and in-situ produced organic matter to the
390 adjacent coastal zone. Following the definition of *NEM*, the trophic status of estuaries can be net
391 heterotrophic (NEM<0) when *HR* exceeds *NPP* or net autotrophic (NEM>0), when *NPP* is larger than
392 *HR* because the burial and export of autochthonous organic matter exceeds the decomposition of
393 river-borne material.

394 The FCO_2 (mol C y^{-1}) is defined as:

$$FCO_2 = \int_0^{365} \int_0^{L} RCO_2(x,t) * B(x)\, dx\, dt \quad (14)$$

395

Biogeosciences Discuss., doi:10.5194/bg-2016-278, 2016
Manuscript under review for journal Biogeosciences
Published: 18 July 2016

$$RCO_2(x,t) = -\mathrm{v_p}(\mathrm{x,t})\left(\left[CO_{2(aq)}\right](x,t) - K_0(x,t) * P_{CO2}(x,t)\right) \quad (15)$$

396

397 where RCO_2 (molC m^{-2} y^{-1}) is the rate of exchange in CO_2 at the air-water interface per unit surface
398 area, v_p is the piston velocity (m y^{-1}) and is calculated according to Regnier et al. (2002) to account
399 for the effect of current velocity and wind speed, [*CO2(aq)*] is the concentration of CO_2 in the
400 estuary (mol m^{-3}), K_0 is Henry's constant of CO_2 in sea water (mol m^{-3} atm^{-1}) and P_{CO2} is the
401 atmospheric partial pressure in CO_2 (atm).

402 The carbon filtering capacity (in %) corresponds to the fraction of the river-borne supply that is lost
403 to the atmosphere and is defined here as the ratio of the net outgassing flux of CO_2 and the total
404 inputs of C, e.g. total carbon expressed as the sum of inorganic and organic carbon species, both in
405 the dissolved and particulate phases.

406 $$CFilt = \frac{FCO_2}{\int_0^{365} Q*[TC]_{riv}\, dt} * 100 \quad (16)$$

407 where $[TC]_{riv}$ denote the total concentrations of C in the riverine inputs.

408 Flux per unit area for FCO_2 and *NEM*, noted $\overline{FCO_2}$ and $\overline{NEM}$, respectively, are defined in mol C m^{-2} y^{-1}
409 and are calculated by dividing the integrated values calculated above by the (idealized) estuarine
410 surface *S*:

411 $$\overline{NEM} = \frac{NEM}{S} * 1000 \quad (17)$$

412 $$\overline{FCO_2} = \frac{FCO_2}{S} * 1000 \quad (18)$$

413 Seasonal values for the biogeochemical indicators are calculated using the same formula as above,
414 but calculate the integral over a seasonal rather than annual timescale (i.e. 3 months).

415

416

Biogeosciences Discuss., doi:10.5194/bg-2016-278, 2016
Manuscript under review for journal Biogeosciences
Published: 18 July 2016

2.6 Model-data comparison

The performance of 1D hydrodynamic and transport models using idealized geometries have been evaluated for a number of estuarine systems exhibiting a wide variety of shapes (Savenije, 2012). In particular, it has been shown that the estuarine salt intrusion can be successfully reproduced using the proposed modeling approach (Savenije 2005; Volta et al., 2014; 2016b). C-GEM's biogeochemistry has also been carefully validated for geometrically contrasting estuarine system in temperate climate zones. Simulations for the Scheldt Estuary (Belgium and the Netherlands), a typical funnel-shaped estuary, were validated through model-data and model-model comparison (Volta et al., 2014; Volta et al., 2016a). Simulations for the Elbe estuary (Germany), a typical prismatic shape estuary draining carbonate terrains, resulting in very high pH was validated against field data (Volta et al., 2016a). In addition, C-GEM carbon budgets have been compared to observation-based estimations for 6 European estuaries discharging in the North Sea (Volta et al., 2016a). This analysis is pursued here by evaluating our model results in the context of estuarine CO_2 evasion estimates along the East coast of the US.

3 Results and discussion

3.1 Spatial variability of estuarine carbon dynamics

Figure 6 presents the spatial distribution of simulated mean annual $\overline{FCO_2}$ and -$\overline{NEM}$ (Fig 6a), as well as FCO_2 and -*NEM* (Fig.6b). In general, mean annual $\overline{FCO_2}$ are about 30% larger than mean annual $\overline{NEM}$, with the exception of six estuaries situated in the North of the coastal segment. Overall, the $\overline{NEM}$ is characterized by smaller system to system variability compared to the $\overline{FCO_2}$ in all regions. In addition, Figure 6 reveals distinct differences across the three coastal segments and highlights the important influence of the estuarine geometry and residence time, as well as the latitudinal temperature gradient on estuarine carbon cycling.

Biogeosciences Discuss., doi:10.5194/bg-2016-278, 2016
Manuscript under review for journal Biogeosciences
Published: 18 July 2016

Overall, $\overline{FCO_2}$ values are the lowest in the NAR (mean flux = 17.3 ± 16.4 mol C m^{-2} y^{-1}; surface weighted average = 23.1 mol C m^{-2} y^{-1}), consistent with previously reported very low values for small estuaries surrounding the Gulf of Maine (Hunt et al., 2010; 2011; table 3). In contrast, $\overline{NEM}$ reveals a regional maximum in the NAR (-51.2 ± 16.6 mol C m^{-2} y^{-1}; surface weighted average = -52.8 mol C m^{-2} y^{-1}). The MAR is characterized by intermediate values for $\overline{FCO_2}$, with a mean flux of 26.3 ± 34.6 mol C m^{-2} y^{-1} (surface weighted average =11.1 mol C m^{-2} y^{-1}) and lowest values for $\overline{NEM}$ (-15.1 ± 14.2 mol C m^{-2} y^{-1}; surface weighted average =-7.4 mol C m^{-2} y^{-1}). This region also shows the largest variability in CO_2 outgassing compared to the NAR and SAR, with the standard deviation exceeding the mean $\overline{FCO_2}$, and individual estimates ranging from 3.9 mol C m^{-2} y^{-1} to 150.8 mol C m^{-2} y^{-1}. This variability is mainly the result of largely variable estuarine surface areas and volumes. Some of the largest East coast estuaries (e.g. Chesapeake and Delaware Bays), as well as some of smallest estuaries (e.g. York River and Hudson River estuaries, Raymond et al., 1997; 2000), are located in this region (table 3 and 4). The maximum values of 150.8 mol C m^{-2} y^{-1} simulated in the MAR are similar to the highest FCO_2 reported in the literature (132.3 mol C m^{-2} y^{-1} for the Tapti estuary in India; Sarma et al., 2012). The SAR is characterized by the highest mean $\overline{FCO_2}$ (46.7 ± 33.0 mol C m^{-2} y^{-1}; surface weighted average = 40.0 mol C m^{-2} y^{-1}) and intermediate $\overline{NEM}$ (-36.8 ± 24.7 mol C m^{-2} y^{-1}; surface weighted average = -31.2 mol C m^{-2} y^{-1}).

The NAR is characterized by a regional minimum in $\overline{FCO_2}$, and only contributes 4.6% to the total FCO_2 of the East coast of the US, owing to the small cumulative surface area available for gas exchange in its 10 estuarine systems. In contrast, the 18 MAR estuaries, with their large relative contribution to the total regional estuarine surface area, account for more than 70% of the total outgassing. Because of their smaller cumulated surface area compared to those of the MAR, the 14 SAR estuaries account for merely 25.3% of the total outgassing despite their regional maximal $\overline{FCO_2}$. A similar, yet slightly less pronounced pattern emerges for the $\overline{NEM}$. The NAR, MAR and SAR respectively contribute 13.7%, 60.7% and 25.6% to the total regional net ecosystem metabolism. The

Biogeosciences Discuss., doi:10.5194/bg-2016-278, 2016
Manuscript under review for journal Biogeosciences
Published: 18 July 2016

comparatively larger relative contribution of the NAR to the total *NEM* as compared to the total FCO_2 can be explained by the importance of the specific aspect ratio for NEM. In the NAR, estuaries are generally characterized by relatively narrow widths and deep-water depths, thus limiting the potential surface area for gas exchange with the atmosphere. However, the relative contribution of each region to the total regional *NEM* and FCO_2 is largely controlled by estuarine surface area. Figure 7 illustrates the cumulative *NEM* (a) and FCO_2 (b) as a function of the cumulative estuarine surface areas. The disproportionate contribution of large estuaries from the MAR translates into a handful of systems (Chesapeake and Delaware Bays and the main tributaries of the former, in particular) contributing to roughly half of the regional *NEM* and FCO_2, in spite of relatively low individual rates per unit surface area. However, the smallest systems (mostly located in the NAR and SAR) nevertheless still contribute a significant fraction to the total regional *NEM* and FCO_2. The 27 smallest systems merely account for less than 10% of the total regional estuarine surface area, yet contribute 38% and 29% to the total regional *NEM* and FCO_2, respectively (Figure 7). This disproportioned contribution can be mainly attributed to their high individual $\overline{FCO_2}$ and $\overline{NEM}$. This is illustrated by the average simulated $\overline{FCO_2}$ for all 27 smallest systems (calculated as the sum of each estuarine CO_2 outgassing per unit surface area divided by the total number of estuarine systems) which is significantly higher (30.2 mol C m^{-2} y^{-1}) than its surface weighted average (14 mol C m^{-2} y^{-1}). Thereby accounting for the disproportionate contribution of very large systems (calculated as the sum of each estuarine CO_2 outgassing divided by the total estuarine surface area across the region).

The contribution of each biogeochemical process to FCO_2 is assessed by evaluating their individual contribution to DIC and ALK changes (see Regnier et al., 2013b). Fig. 8a presents the contribution of the annually integrated *NEM*, nitrification and evasion of supersaturated, DIC enriched riverine waters to the total outgassing for each system, as well as for individual regions of the domain. Model results reveal that, regionally, the *NEM* supports about 50% of the estuarine CO_2 outgassing, while

Biogeosciences Discuss., doi:10.5194/bg-2016-278, 2016
Manuscript under review for journal Biogeosciences
Published: 18 July 2016

490 nitrification and riverine DIC inputs sustain about 17% and 33% of the CO_2 emissions, respectively.
491 Nitrification, a process triggered by the transport and/or production of NH_4 in oxygenated waters,
492 favors outgassing through its effect on pH, which shifts the acid-base equilibrium of carbonate
493 species and increases the CO_2 concentration. In addition, the *NEM* is almost exclusively controlled by
494 aerobic degradation rates because the contribution of denitrification and NPP to the net ecosystem
495 balance is small.

496 The relative significance of the three processes described above shows important spatial variability.
497 In the NAR, oversaturated riverine waters and NEM respectively sustain 50% and 44% of the
498 outgassing within the sub-region, while nitrification is of minor importance (6%). In the MAR, the
499 contribution of riverine DIC inputs is significantly lower (~30%) and the main contribution to the
500 outgassing is *NEM* (~50%); nitrification accounting for slightly less than 20% of the outgassing. In the
501 SAR, the riverine contribution is even lower (~20%), and the outgassing is mainly attributed to the
502 *NEM* (~55%) and nitrification (~25%). Therefore, although the model results reveal significant
503 variability across individual systems, a clear latitudinal trend in the contribution to the total FCO_2
504 emerge from the analysis; the importance of oversaturated riverine water decreasing from North to
505 South, while *NEM* and nitrification increase along the same latitudinal gradient. The increasing
506 relative importance of estuarine biogeochemical processes over riverine DIC inputs as drivers of
507 FCO_2 along the North-South gradient is largely driven by increasing temperatures from North to
508 South, especially in the SAR region (Table S1).

509 Contrasting patterns across the 3 regions can also be observed with respect to carbon filtering
510 capacities, *CFilt* (Fig 8b). In the NAR, over 90% of the riverine carbon flux is exported to the coastal
511 ocean. However, in the MAR, the high efficiency of the largest systems in processing organic carbon
512 results in a regional *CFilt* that exceeds 50%. This contrast between the NAR and the MAR and its
513 potential implication for the carbon dynamics of the adjacent continental shelf waters has already
514 been discussed by Laruelle et al. (2015). In the NAR, short estuarine residence results in a much

Biogeosciences Discuss., doi:10.5194/bg-2016-278, 2016
Manuscript under review for journal Biogeosciences
Published: 18 July 2016

lower removal of riverine carbon by degassing compared to the MAR. Laruelle et al. (2015) suggested that this process could contribute to the weaker continental shelf carbon sink adjacent to the NAR, compared to the MAR. In the SAR, most estuaries remove between 40% and 65% of the carbon inputs. The high temperatures observed and resulting accelerated biogeochemical process rates in this region favor the degradation of organic matter and contribute to increase the estuarine filtering capacity for carbon. However, in the SAR, a large fraction of the OC loads is derived from adjacent salt marshes located along the estuarine salinity gradients, thereby reducing the overall residence time of OC within the systems. The filtering capacity of the riverine OC alone, which transits through the entire estuary, would thus be higher than the one calculated here. As a consequence, highest C retention rates are expected in warm tidal estuaries devoid of salt marshes or mangroves (Cai, 2011).

3.2 Seasonal variability of estuarine carbon dynamics

Carbon dynamics in estuaries of the US East coast not only show a marked spatial variability, but also vary on the seasonal timescale. Table 5 presents the seasonal distribution of *NEM* and FCO_2 for each sub-region. In the NAR, a strong seasonality is simulated for the *NEM* and the summer period contributes more than a third to the annually integrated value. The outgassing reveals a lower seasonal variability and is only slightly higher than summer outgassing during fall and lower during spring. In the MAR, summer contributes more to the *NEM* (>28% of the yearly total) than any other season, but seasonality is less pronounced than in the NAR. Here, FCO_2 is largest in winter and particularly low during summer. In the SAR, summer accounts for 30 % of the NEM, while spring contributes 21 %. FCO_2 is relatively constant throughout the year suggesting that seasonal variations in carbon processing decrease towards the lower latitudes in the SAR. This is partly related to the low variability in river discharge throughout the year in lower latitudes (Table S1). In riverine dominated systems with low residence times, such as, for instance, the Altamaha River estuary, the CO_2 exchange at the air-water interface is mainly controlled by the river discharge because the time required to degrade the entire riverine organic matter flux exceeds the transit time of OC through

Biogeosciences Discuss., doi:10.5194/bg-2016-278, 2016
Manuscript under review for journal Biogeosciences
Published: 18 July 2016

541 the estuary. Therefore, the riverine sustained outgassing is highest during the spring peak discharge
542 periods. In contrast, the seasonal variability in FCO_2 in long-residence, marine-dominated systems
543 with large marsh areas (e.g. Sapelo and Doboy Sound) is essentially controlled by seasonal
544 temperature variations. Its maximum is reached during summer when marsh plants are dying and
545 decomposing, as opposed to spring when marshes are in their productive stage (Jiang et al., 2008).
546 These contrasting seasonal trends have already been reported for different estuarine systems in
547 Georgia, such as the Altamaha Sound, the Sapelo Sound and the Doboy Sound (Cai, 2011). At the
548 scale of the entire East coast of the US, the seasonal trends in *NEM* reveal a clear maximum in
549 summer and minimal values during autumn and winter. The seasonality of FCO_2 is much less
550 pronounced because the outgassing of oversaturated riverine waters throughout the year
551 contributes to a large fraction of the FCO_2 and dampens the effect of the temperature dependent
552 processes (*NEM* and denitrification). In our simulations, the competition between temperature and
553 river discharge is the main driver of the seasonal estuarine carbon dynamics is. When discharge
554 increases, the carbon loads increase proportionally and the residence time within the system
555 decreases, consequently limiting an efficient degradation of organic carbon input fluxes. In warm
556 regions like the SAR, the temperature is sufficiently high all year round to sustain high C processing
557 rates and this explains the reduced seasonal variability in NEM.
558
559 **3.3 Regional carbon budget: a comparative analysis**

560 The annual carbon budget for the entire East coast of the US is summarized in fig 9a. The total
561 carbon input to estuaries along the East coast of the US is 4.6 Tg C y^{-1}, of which 42% arrives in
562 organic form and 58% in inorganic form**.** Of this total input, saltmarshes contribute 0.6 Tg C yr^{-1},
563 which corresponds to about 14% of the total carbon loads and 32% of the organic loads in the
564 region. The relative contribution of the saltmarshes to the total carbon input increases towards low
565 latitudes and is as high as 60% in the SAR region. Model results suggest that 2.7 Tg C y^{-1} is exported
566 to the continental shelf (25% as TOC and 75% as DIC), while 1.9 Tg C y^{-1} is emitted to the

Biogeosciences Discuss., doi:10.5194/bg-2016-278, 2016
Manuscript under review for journal Biogeosciences
Published: 18 July 2016

atmosphere. The overall carbon filtering capacity of the region thus equals 41% of the total carbon entering the 47 estuarine systems (river + saltmarshes). Because of the current lack of a benthic module in C-GEM, the water column carbon removal occurs entirely in the form of CO_2 outgassing and does not account for the potential contribution of carbon burial in sediments. The estimated estuarine carbon retention presented here is thus likely a lower bound estimate. Reported to the modeled surface area of the region, the total FCO_2 of 1.9 Tg C y^{-1} translates into a mean air water CO_2 flux of about 14 mol C m^{-2} y^{-1}. This value is slightly higher than the estimate of 10.8 mol C m^{-2} y^{-1} calculated by Laruelle et al., (2013) on the basis of local $\overline{FCO_2}$ estimates assumed to be representative of yearly averaged conditions (see section 2.1). The latter was calculated as the average of 13 annual $\overline{FCO_2}$ values reported in the literature (table 3), irrespective of the size of the systems. This approach is useful and widely used to derive regional and global carbon budget (Borges et al., 2005; Laruelle et al., 2010; Chen et al., 2013). However, it may lead to potentially significant errors (Volta et al., 2016a) due to the uncertainty introduced by the spatial interpolation of local measurements to large regional surface areas, while useful and widely used to derive regional and global carbon budgets.

Regional C budgets are sparse. To our knowledge, the only other published regional assessment of the estuarine carbon and CO_2 dynamics comes from a relatively well studied region: the estuaries flowing into the North Sea in Western Europe (Fig. 9b). This budget was calculated using a similar approach (Volta 2016a) and thus provides an ideal opportunity for a comparative assessment of C cycling in these regions. However, it is important to note that there are also important differences in the applied model approaches and those differences should be taken into account when comparing the derived budgets. In particular, the NW European study is based on a simulation of the 6 largest systems only (Elbe, Scheldt, Thames, Ems, Humber and Weser), accounting for about 40% for the riverine carbon loads of the region. It assumes that the intensity of carbon processing and evasion in all other smaller estuaries discharging into the North Sea (16 % of the carbon loads) can be

Biogeosciences Discuss., doi:10.5194/bg-2016-278, 2016
Manuscript under review for journal Biogeosciences
Published: 18 July 2016

592 represented by the average of the 6 largest system simulation results. In addition, the Rhine-Meuse
593 system, which alone accounts for 44% of the carbon riverine inputs of the region, was treated as a
594 passive conduit with respect to carbon due to its very short freshwater residence time (Abril et al.,
595 2002). The contribution of saltmarshes to the regional carbon budget was also ignored because their
596 total surface area is much smaller than along the US East coast (Regnier et al., 2013b). Another
597 important difference is the inclusion of seasonality in the present study while the budget calculated
598 for the North Sea is derived from yearly average conditions (Volta et al., 2016a).

599 Overall, although both regions receive similar amounts of C from rivers (4.6 Tg C y^{-1} and 5.9 Tg C y^{-1}
600 for the East coast of the US and the North Sea, respectively), they reveal significantly different C
601 filtering capacities. While the estuaries of the East coast of the US filter 41% of the riverine TC loads,
602 those from the North Sea only remove 8% of the terrestrial-derived material. This is partly due to the
603 large amounts of carbon transiting through the 'passive' Rhine-Meuse system. The regional filtering
604 capacity is higher (15%) when this system is excluded from the analysis. However, even when
605 neglecting this system, significant differences in filtering efficiencies between both regions remain.
606 FCO_2 from the North Sea estuaries (0.5 Tg C y^{-1}) is significantly lower than the 1.9 Tg C y^{-1} computed
607 for the East coast of the US. The reason for the lower evasion rate in NW European estuaries is
608 essentially twofold. First, the total cumulative surface area available for gas exchange is significantly
609 lower along the North Sea, in spite of comparable flux densities calculated using the entire estuarine
610 surface areas of both regions (14 mol C m^{-2} y^{-1} and 23 mol C m^{-2} y^{-1} for the East coast of the US and
611 the North Sea, respectively). Second, although the overall riverine carbon loads are comparable in
612 both regions (Fig 9), the ratio of organic to inorganic matter input is much lower in the North Sea
613 area because of the regional lithology is dominated by carbonate rocks and mixed sediments that
614 contain carbonates (Dürr et al., 2005; Hartmann et al., 2012). As a consequence, TOC represents less
615 than 20% of the riverine loads and only 10% of the carbon exported to the North Sea. In both
616 regions, however, the increase of the inorganic to organic carbon ratio between input and output is
617 sustained by a negative NEM (Fig.9). Although the ratios themselves may significantly vary from a

Biogeosciences Discuss., doi:10.5194/bg-2016-278, 2016
Manuscript under review for journal Biogeosciences
Published: 18 July 2016

618 region of the world to the other as evidenced by these two studies, a NEM driven increase of the
619 inorganic fraction within carbon load along the estuarine axis is consistent with the global estuarine
620 carbon budget proposed by Bauer et al. (2013). In the East coast of the US, the respiration of riverine
621 OC within the estuarine filter is partly compensated by OC inputs from marshes and mangroves in
622 such a way that the input and export IC/OC ratios are closer than in the North Sea region.

623 **3.4 Towards predictors of the estuarine carbon processing**

624 The mutual dependence between geometry and transport in tidal estuaries and, ultimately, their
625 biogeochemical functioning (Savenije, 1992; Volta et al., 2014) allows relating easily extractable
626 parameters linked to their shape or their hydraulic properties to biogeochemical indicators. In this
627 section, we explore the relationships between such simple physical parameters and indicators of the
628 estuarine carbon processing $\overline{NEM}$, $\overline{FCO_2}$ and *CFilt*. In order to account for the effect of temperature
629 on C dynamics, -$\overline{NEM}$ and $\overline{FCO_2}$ are also normalized to the same temperature (arbitrarily chosen to
630 be 0 degree). These normalized values are obtained by dividing -$\overline{NEM}$ and $\overline{FCO_2}$ by a Q_{10} function
631 *f(T)* (see Volta et al., 2014). The three indicators are then investigated as a function of the ratio
632 between the estuarine surface *S* and the seasonal river discharge *Q*. The surface area is calculated
633 from the estuarine width and length, as described by equation 2, in order to use a parameter which
634 is potentially applicable to other regions for which direct estimates of the real estuarine surface area
635 is not available. Since the fresh water residence time of a system is obtained by dividing volume by
636 river discharge, the S/Q ratio is also intimately linked to residence time. Here, we choose to exclude
637 the estuarine depth from the analysis because this variable cannot be easily quantified from maps or
638 remote sensing images and would thus compromise the applicability of a predictive relationship on
639 the global scale. However, from dimensional analysis, S/Q can be viewed as a water residence time
640 normalized to meter depth of water. As shown by equation 3, *S* only requires constraining *B0* and
641 width convergence length *b*, two parameters that can readily be extracted from the Google Earth
642 engine. Global database of river discharges, as for instance RivDIS (Vörösmarty et al., 1996) are also

Biogeosciences Discuss., doi:10.5194/bg-2016-278, 2016
Manuscript under review for journal Biogeosciences
Published: 18 July 2016

643 available in such a way that the S/Q ratio can potentially be extracted for all estuaries around the
644 globe.

645 Figure 10a reveals that small values of S/Q are associated with the most negative $\overline{NEM}$ / $f(T)$. The
646 magnitude of the $\overline{NEM}$ then exponentially decreases with increasing values of S/Q. Estuaries
647 characterized by small values of *S/Q* are mainly located in the NAR sub-region and correspond to
648 small surface area, and thus short residence time systems. It is possible to quantitatively relate -
649 $\overline{NEM}$ /$f(T)$ and S/Q through a power law function (y = 25.85 $x^{-0.64}$ with a r^2 = 0.82). The coefficient
650 of determination remains the same when excluding estuaries from the NAR region and the equation
651 itself is not significantly different, although those estuaries on their own do not display any
652 statistically significant trend (table 6). The decrease in the intensity of the net ecosystem metabolism
653 in larger estuaries (Fig 6), characterized by high S/Q ratios, can be related to the extensive
654 consumption of the organic matter pool during its transit through the estuarine filter. However,
655 when reported to the entire surface area of the estuary, larger systems (with high values of S/Q) still
656 reveal the most negative surface integrated *NEM* (fig 10b). It can also be noted that some estuaries
657 from the NAR region display very low values of *–NEM*. These data points correspond to fall and
658 winter simulations for which the temperature was relatively cold (<5 °C) and biogeochemical
659 processing was very low.

660 The response of $\overline{FCO_2}/f(T)$ to S/Q is comparable to that of -$\overline{NEM}/f(T)$ (Fig 10c), with lower values
661 of $\overline{FCO_2}$ observed for high values of S/Q. However, for S/Q < 3 days m^{-1}, the $\overline{FCO_2}$ values are very
662 heterogeneous and contain many, low $\overline{FCO_2}$ outliers from the NAR region. These data points
663 generally correspond to low water temperature conditions which keep pCO_2 low, even if the system
664 generates enough CO_2 internally via NEM. Thus, the well-documented correlation between $\overline{NEM}$
665 and $\overline{FCO_2}$ (Maher and Eyre, 2012) does not seem to hold for systems with very short residence
666 times. For systems with S/Q > 3 days m^{-1}, we obtain a regression FCO_2 = -0.64 x *NEM* + 5.96 with a r^2
667 of 0.46, which compares well with the relation FCO_2 = -0.42 x *NEM* + 12 proposed by Maher and Eyre

Biogeosciences Discuss., doi:10.5194/bg-2016-278, 2016
Manuscript under review for journal Biogeosciences
Published: 18 July 2016

(2012) whom used 24 seasonal estimates from small Australian estuaries. Discharge is the main FCO_2 driver in riverine dominated systems, while interactions with marshes are driving the outgassing in marine dominated systems surrounded by marshes. Net aquatic biological production (NEM being negative or near 0) in large estuaries (with large S/Q) is another important reason for low FCO_2 in such systems. For example, despite the higher CO_2 degassing flux in the upper estuary of the Delaware, strong biological CO_2 uptake in the mid-bay and near zero NEM in the lower bay result in a much lower FCO_2 for the entire estuary (Joesoef et al. 2015). In systems with S/Q < 3 days m^{-1}, the short residence time prevents the excess CO_2 of oversaturated water from being entirely exchanged with the atmosphere and simulations reveal that the estuarine waters are still oversaturated in CO_2 at the estuarine mouth. Thus, the inorganic carbon, produced by the decomposition of organic matter, is not outgassed within the estuary but exported to the adjacent continental shelf waters. This result is consistent with the observation-based hypothesis of Laruelle et al. (2015) for the NAR estuaries. As a consequence of the distinct behavior of short residence time systems, the coefficient of determination of the best-fitted power law function relating $\overline{FCO_2}$ and S/Q is only significant if NAR systems are excluded ($y = 31.64\ x^{-0.58}$ with a $r^2 = 0.70$).

Finally, Figure 10e reports the simulated mean seasonal carbon filtering capacities as a function of the depth normalized residence time. Not surprisingly, and in overall agreement with previous studies on nutrient dynamics in estuaries (Nixon et al., 1996), the carbon filtering capacity increases with S/Q. The best statistical relation between *CFilt* and S/Q is obtained when including all 3 regions, resulting in $r^2 = 0.70$ ($y = 40.64 \log_{10}(x) + 11.84$). Very little C removal occurs in systems with S/Q < 1 day m^{-1}. For systems characterized by longer depth-normalized residence times, *CFilt* increases regularly, and reaches 100% for S/Q > 100 day m^{-1}. Such high values are only observed for very large estuaries from the MAR region (Delaware and Chesapeake Bays); the majority of our systems had an *S/Q* range between 1 and 100 day m^{-1}. The quantitative assessment of estuarine filtering capacities is further complicated by the complex interplay of estuarine and coastal processes. Episodically, marked spatial variability in concentration gradients near the estuarine mouth may lead to a reversal

Biogeosciences Discuss., doi:10.5194/bg-2016-278, 2016
Manuscript under review for journal Biogeosciences
Published: 18 July 2016

694 of net material fluxes from coastal waters into the estuary (Regnier at al., 1998; Arndt et al. 2011).
695 Our results show that this feature is particularly significant for estuaries with a large width at the
696 mouth and short convergence length (funnel shaped or 'Bay type' systems). These coastal nutrient
697 and carbon inputs influence the internal estuarine C dynamics and lead to filtering capacities that
698 can exceed 100%. This feature is particularly significant in summer, when riverine inputs are low and
699 the marine material is intensively processed inside the estuary.

700 Previous work investigated the relationship between fresh water residence time and nutrient
701 retention (Nixon et al., 1996; Arndt et al., 2011; Laruelle, 2009). These studies, however, were
702 constrained by the scarcity of data. For instance, the pioneering work of Nixon et al. (1996) only
703 relied on a very limited number (<10) of quite heterogeneous coastal systems, all located along the
704 North Atlantic. Here, our modeling approach allows us to generate 172 (43 x 4) data points, each
705 representing a system-scale biogeochemical behavior. Together, this database spans the entire
706 spectrum of estuarine settings and climatic conditions found along the East coast of the US. In
707 addition, the ratio S/Q used as master variable for predicting temperature normalized -$\overline{NEM}$, $\overline{FCO_2}$
708 and *CFilt* only requires a few easily accessible geometric parameters (B0, b and L) and an estimate of
709 the river discharge. While it is difficult to accurately predict $\overline{FCO_2}$ for small systems such as those
710 located in the NAR region, the relationships found are quite robust for systems in which S/Q > 3 days
711 m^{-1}. Most interestingly, *CFilt* values reveal a significant correlation with S/Q and could be used in
712 combination with global riverine carbon delivery estimates such as GlobalNews 2 (Mayorga et al.,
713 2010) to constrain the estuarine CO_2 evasion and the carbon export to the coastal ocean at the
714 continental and global scales.

715 **4. Conclusions**

716 This study presents the first complete estuarine carbon budget for the East coast of the US using a
717 modeling approach. The structure of the model C-GEM relies on a restricted number of readily
718 available global datasets to constrain boundary conditions and limits the number of geometrical and

Biogeosciences Discuss., doi:10.5194/bg-2016-278, 2016
Manuscript under review for journal Biogeosciences
Published: 18 July 2016

physical parameters to be constrained. Our simulations predict a total CO_2 outgassing of 1.9 Tg C y^{-1} for all tidal estuaries of the East coast of the US. This quantification accounts for the seasonality in estuarine carbon processing as well as for distinct individual behaviors among estuarine types (marine or river dominated). The total carbon output to the coastal ocean is estimated at 2.7 TgC y^{-1}, and the carbon filtering capacity with respect to riverine, marshes and mangrove inputs is thus on the order of 40%. This value is significantly higher than the recently estimated C filtering capacity for estuaries surrounding the North Sea using a similar approach (Volta et al., 2016a), mainly because the surface area available for gas exchange and the draining lithology limits the CO_2 evasion in the NW European systems. At the regional scale of the US East coast estuaries, net heterotrophy is the main driver (50%) of the CO_2 outgassing, followed by the ventilation of riverine supersaturated waters entering the estuarine systems (32%) and nitrification (18%). The dominant mechanisms for the gas exchange and the resulting carbon filtering capacities nevertheless reveal a clear latitudinal pattern, which reflects the shapes of estuarine systems, climatic conditions and dominant land-use characteristics.

Our model results are used to derive predictive relationships relating the intensity of the area-based Net Ecosystem Metabolism ($\overline{NEM}$), air-water CO_2 exchange ($\overline{FCO_2}$) and the carbon filtering capacity (*CFilt*) to the depth normalized residence time, expressed as the ratio of the estuarine surface area to the river discharge. In the future, such simple relationships relying on readily available geometric and hydraulic parameters could be used to quantify carbon processing in areas of the world devoid of direct measurements. In regions with better data coverage, such as the one investigated here, our study highlights that the regional-scale quantification, attribution, and prediction of estuarine biogeochemical cycling are now at reach.

5. Acknowledgements

G. G. Laruelle is Chargé de recherches du F.R.S.-FNRS at the Université Libre de Bruxelles. The research leading to these results has received funding from the European Union's Horizon 2020

744 research and innovation programme under the Marie Sklodowska-Curie grant agreement No 643052
745 (C-CASCADES project). The authors thank V. L. Mulder for her thorough reading of the manuscript
746 upon submission.

747

748 **References:**

749 Abril, G., Nogueira, M., Etcheber, H., Cabeçadas, G., Lemaire, E., and Brogueira, M.J.: Behaviour of
750 organic carbon in nine contrasting European estuaries. Estuar. Coast. Shelf Sci., 54, 241-262,
751 2002.
752 Antonov, J.I., Seidov, D., Boyer, T.P., Locarnini, R.A., Mishonov, A.V., Garcia, H.E., Baranova, O.K.,
753 Zweng, M.M., and Johnson, D.R.: World Ocean Atlas 2009, Volume 2: Salinity. S., 2010.
754 Arndt, S., Vanderborght, J.P., and Regnier, P.: Diatom growth response to physical forcing in a
755 macrotidal estuary: Coupling hydrodynamics, sediment transport, and biogeochemistry.
756 Journal of Geophysical Research C: Oceans, 112(5), 2007.
757 Arndt, S., Regnier, P., and Vanderborght, J.P.: Seasonally-resolved nutrient export fluxes and filtering
758 capacities in a macrotidal estuary. Journal of Marine Systems, 78(1), 42-58, 2009.
759 Arndt, S., Lacroix, G., Gypens, N., Regnier, P., and Lancelot, C.: Nutrient dynamics and phytoplankton
760 development along an estuary-coastal zone continuum: A model study. Journal of Marine
761 Systems, 84(3-4), 49-66, 2011.
762 Atlas, R., Hoffman, R.N., Ardizzone, J., Leidner, S.M., Jusem, J.C., Smith, D.K. and Gombos, D.: A
763 cross-calibrated, multiplatform ocean surface wind velocity product for meteorological and
764 oceanographic applications. Bulletin of the American Meteorological Society, 92(2), 157-174,
765 2011.
766 Bauer, J.E., Cai, W.J., Raymond, P.A., Bianchi, T.S., Hopkinson, C.S., and Regnier, P.A.G.: The changing
767 carbon cycle of the coastal ocean. Nature, 504(7478), 61-70, 2013.
768 Beusen, A.H.W., Bouwman, A.F., Dürr, H.H., Dekkers, A.L.M., and Hartmann, J.: Global patterns of
769 dissolved silica export to the coastal zone: Results from a spatially explicit global model.
770 Global Biogeochemical Cycles, 23, GB0A02, doi:10.1029/2008GB003281, 2009.
771 Billen, G., Thieu, V., Garnier, J., and Silvestre, M.: Modelling the N cascade in regional waters: The
772 case study of the Seine, Somme and Scheldt rivers, Agr. Ecosyst. Environ., 133, 234–246,
773 2009.
774 Borges, A.V., Delille, B., and Frankignoulle, M.: Budgeting sinks and sources of CO_2 in the coastal
775 ocean: Diversity of ecosystems counts. Geophys. Res. Lett., 32(14), L14601, 2005.
776 Borges, A.V., and Abril, G.: Carbon Dioxide and Methane Dynamics in Estuaries. In: E. Wolanski and
777 D.S. McLusky (Editors), Treatise on Estuarine and Coastal Science. Academic Press, Waltham,
778 pp. 119–161, 2012.
779 Bricker, S., Longstaff, B., Dennison, W., Jones, A., Boicourt, K., Wicks, C., and Woerner, J.: Effects of
780 Nutrient Enrichment In the Nation's Estuaries: A Decade of Change, NOAA, MD, 2007.
781 Brock, T.D.: Calculating solar radiation for ecological studies. Ecological Modelling, 14(1-2), 1-19,
782 1981.
783 Caffrey, J.: Factors controlling net ecosystem metabolism in U.S. estuaries. Estuaries, 27(1), 90-101,
784 2004.
785 Cai, W.J., and Wang, Y.: The chemistry, fluxes, and sources of carbon dioxide in the estuarine waters
786 of the Satilla and Altamaha Rivers, Georgia. Limnology and Oceanography, 43(4), 657-668,
787 1998.

788 Cai, W.J., Pomeroy, L.R., Moran, M.A., and Wang, Y.: Oxygen and carbon dioxide mass balance for
789 the estuarine-intertidal marsh complex of five rivers in the southeastern U.S. Limnology and
790 Oceanography, 44, 639-649, 1999.
791 Cai, W.J.: Estuarine and coastal ocean carbon paradox: CO_2 sinks or sites of terrestrial carbon
792 incineration? Ann. Rev. Mar. Sci., 3, 123-145, 2011.
793 Chen, C.-T.A., Huang, T.-H., Fu, Y.-H., Bai, Y., and He, X.: Strong sources of CO2 in upper estuaries
794 become sinks of CO2 in large river plumes. Current Opinion in Environmental Sustainability,
795 4(2), 179-185, 2012.
796 Chen, C.-T. A., Huang, T.-H., Chen, Y.-C., Bai, Y., He, X., and Kang, Y.: Air-sea exchanges of CO2 in the
797 world's coastal seas, Biogeosciences, 10, 6509–6544, doi:10.5194/bg-10-6509-2013, 2013.
798 Dai, T., and Wiegert, R.G.: Estimation of the primary productivity of Spartina alterniflora using a
799 canopy model. Ecography, 19(4), 410-423, 1996.
800 DuFore, C. M.: Spatial and Temporal Variations in the Air-Sea Carbon Dioxide Fluxes of Florida Bay,
801 Gratuate School Thesis, University of South Florida, 2012.
802 Dürr, H.H., Meybeck, M., and Dürr, S.H.: Lithological composition of the Earth's continental surfaces
803 derived from a new digital map emphasizing riverine material transfer. Glob. Biogeochem.
804 Cycles 19 (4), GB4S10, 2005.
805 Dürr, H.H., Laruelle, G.G., van Kempen, C.M., Slomp, C.P., Meybeck, M., and Middelkoop, H.:
806 Worldwide Typology of Nearshore Coastal Systems: Defining the Estuarine Filter of River
807 Inputs to the Oceans. Estuaries and Coasts, 34(3), 441-458, 2011.
808 EPA (2009). "1970 - 2008 Average annual emissions, all criteria pollutants in MS Excel." National
809 Emissions Inventory (NEI) Air Pollutant Emissions Trends Data. Office of Air Quality Planning
810 and Standards. Available online at <http://www.epa.gov/ttn/chief/trends/index.html>
811 Fekete, B.M., Vörösmarty, C.J., and Grabs, W.: High-resolution fields of global runoff combining
812 observed river discharge and simulated water balances. Global Biogeochemical Cycles, 16(3),
813 15-1, 2002.
814 Fischer, H. B.: Mixing and Dispersion in Estuaries, Annu. Rev. Fluid Mech., 8, 107–133,
815 1976.Friedrichs, M.A.M., and Hofmann, E.E.: Physical control of biological processes in the
816 central equatorial Pacific Ocean. Deep-Sea Research Part I: Oceanographic Research Papers,
817 48(4), 1023-1069, 2001.
818 Garcia, H.E., Locarnini, R.A., Boyer, E.W., Antonov, A., Baranova, O.K., Zweng, M.M., and Johnson,
819 D.R.: World Ocean Atlas 2009, Volume 3: Dissolved Oxygen, Apparent Oxygen Utilization,
820 and Oxygen Saturation, 2010a.
821 Garcia, H.E., Locarnini, R.A., Boyer, E.W., Antonov, J.I., Baranova, O.K., Zweng, M.M., and Johnson,
822 D.R.: World Ocean Atlas 2009, Volume 4: Nutrients (phosphate, nitrate, silicate), 2010b.
823 Harrison, J.A., Caraco, N., and Seitzinger, S.P.: Global patterns and sources of dissolved organic
824 matter export to the coastal zone: Results from a spatially explicit, global model. Global
825 Biogeochemical Cycles, 19(4), GB4S03, doi:10.1029/2004GB002357, 2005.
826 Hartmann, J., Jansen, N., Dürr, H.H., Kempe, S., and Köhler, P.: Global CO_2 consumption by chemical
827 weathering: What is the contribution of highly active weathering regions? Global Planet.
828 Change, 69(4), 185-194, 2009.
829 Hartmann, J., Dürr, H.H., Moosdorf, N., Meybeck, M., and Kempe, S.: The geochemical composition
830 of the terrestrial surface (without soils) and comparison with the upper continental crust.
831 Int. J. Earth Sci. 101, 365-376, 2012.
832 Herrmann, M., Najjar, R.G., Kemp, W.M., Alexander, R.B., Boyer, E.W., Cai, W.-J., Griffith, P.C.,
833 Kroeger, K.D., McCallister, S.L., and Smith, R.A.: Net ecosystem production and organic
834 carbon balance of U.S. East Coast estuaries: A synthesis approach, Global Biogeochem.
835 Cycles, 29, doi:10.1002/2013GB004736, 2015.
836 Hofmann, A.F., Soetaert, K., and Middelburg, J.J.: Present nitrogen and carbon dynamics in the
837 Scheldt estuary using a novel 1-D model. Biogeosciences, 5(4), 981-1006, 2008.

838 Hunt, C. W., Salisbury, J. E., Vandemark, D., and McGillis, W.: Contrasting Carbon Dioxide Inputs and
839 Exchange in Three Adjacent New England Estuaries. Estuar. Coast., 34, 68–77,
840 doi:10.1007/s12237-010-9299-9, 2010.
841 Hunt, C.W., Salisbury, J.E., Vandemark, D., and McGillis, W.: Contrasting Carbon Dioxide Inputs and
842 Exchange in Three Adjacent New England Estuaries. Estuaries and Coasts, 34(1), 68-77, 2011.
843 Ippen, A.T., and Harleman, D.R.F.: One-dimensional Analysis of Salinity Intrusion in Estuaries,
844 Technical Bulletin No. 5, Committee on Tidal Hydraulics, Corps of Engineers, US Army,
845 Vicksburg, 1961.
846 Jiang, L.Q., Cai, W.J., and Wang, Y.: A comparative study of carbon dioxide degassing in river- and
847 marine-dominated estuaries. Limnology and Oceanography, 53(6), 2603-2615, 2008.
848 Jiang, L.-Q., Cai, W.-J., Wang, Y., and Bauer, J. E.: Influence of terrestrial inputs on continental shelf
849 carbon dioxide, Biogeosciences, 10, 839–849, doi:10.5194/bg-10-839-2013, 2013.
850 Joesoef, A., Huang, W.-J., Gao, Y., and Cai, W.-J.: Air–water fluxes and sources of carbon dioxide in
851 the Delaware Estuary: spatial and seasonal variability, Biogeosciences, 12, 6085-6101,
852 doi:10.5194/bg-12-6085-2015, 2015.
853 Kent, B.H.: Turbulent diffusion in a Sectionally Homogeneous Estuary, Technical Report 16,
854 Chesapeake Bay Institute, John Hopkins, University, Baltimore, 1958.
855 Key, R.M., Kozyr, A., Sabine, C.L., Lee, K., Wanninkhof, R., Bullister, J.L., Feely, R.A., Millero, F.J.,
856 Mordy, C., and Peng, T.H.: A global ocean carbon climatology: Results from Global Data
857 Analysis Project (GLODAP). Global Biogeochemical Cycles, 18(4), 1-23, 2004.
858 Laruelle, G.G.: Quantifying nutrient cycling and retention in coastal waters at the global scale, Ph D
859 dissertation, Utrecht University, 2009.
860 Laruelle, G. G., Regnier, P., Ragueneau, O., Kempa, M., Moriceau, B., Ni Longphuirt, S., Leynaert, A.,
861 Thouzeau, G., and Chauvaud, L.: Benthic-pelagic coupling and the seasonal silica cycle in the
862 Bay of Brest (France): new insights from a coupled physical-biological model, Mar. Ecol.-
863 Prog. Ser., 385, 15–32, 2009.
864 Laruelle, G.G., Dürr, H.H., Slomp, C.P., and Borges, A.V.: Evaluation of sinks and sources of CO_2 in the
865 global coastal ocean using a spatially-explicit typology of estuaries and continental shelves.
866 Geophys. Res. Lett., 37(15), L15607, doi:10.1029/2010GL043691, 2010.
867 Laruelle, G.G., Dürr, H.H., Lauerwald, R., Hartmann, J., Slomp, C.P., Goossens, N., and Regnier, P.A.G.:
868 Global multi-scale segmentation of continental and coastal waters from the watersheds to
869 the continental margins. Hydrol. Earth Syst. Sci., 17(5), 2029-2051, 2013.
870 Laruelle, G.G., Lauerwald, R., Rotschi, J. Raymond, P.A., and Regnier, P.: Seasonal response of air-
871 water CO2 exchange along the land-ocean aquatic continuum of the northeast North
872 American coast. Biogeosci. 12, 1447-1458, 2015.
873 Lauerwald, R., Hartmann, J., Moosdorf, N., Kempe, S., and Raymond, P.A.: What controls the spatial
874 patterns of the riverine carbonate system? — A case study for North America. Chemical
875 Geology, 337–338, 114-127, 2013.
876 Leonard, B.: Third-Order Upwinding as a Rational Basis for Computational Fluid Dynamics, in:
877 Computational Techniques and Applications: CTAC-83, edited by: Noye J. and Fletcher C. A.
878 J., Elsevier, North-Holland, 1984.
879 Le Quéré, C., Peters, G. P., Andres, R. J., Andrew, R. M., Boden, T. A., Ciais, P., Friedlingstein, P.,
880 Houghton, R. A., Marland, G., Moriarty, R., Sitch, S., Tans, P., Arneth, A., Arvanitis, A., Bakker,
881 D. C. E., Bopp, L., Canadell, J. G., Chini, L. P., Doney, S. C., Harper, A., Harris, I., House, J. I.,
882 Jain, A. K., Jones, S. D., Kato, E., Keeling, R. F., Klein Goldewijk, K., Körtzinger, A., Koven, C.,
883 Lefèvre, N., Maignan, F., Omar, A., Ono, T., Park, G.-H., Pfeil, B., Poulter, B., Raupach, M. R.,
884 Regnier, P., Rödenbeck, C., Saito, S., Schwinger, J., Segschneider, J., Stocker, B. D., Takahashi,
885 T., Tilbrook, B., van Heuven, S., Viovy, N., Wanninkhof, R., Wiltshire, A., and Zaehle, S.:
886 Global carbon budget 2013, Earth Syst. Sci. Data, 6, 235-263, doi:10.5194/essd-6-235-2014,
887 2014.

888 Le Quéré, C., Moriarty, R., Andrew, R. M., Canadell, J. G., Sitch, S., Korsbakken, J. I., Friedlingstein, P.,
889 Peters, G. P., Andres, R. J., Boden, T. A., Houghton, R. A., House, J. I., Keeling, R. F., Tans, P.,
890 Arneth, A., Bakker, D. C. E., Barbero, L., Bopp, L., Chang, J., Chevallier, F., Chini, L. P., Ciais, P.,
891 Fader, M., Feely, R. A., Gkritzalis, T., Harris, I., Hauck, J., Ilyina, T., Jain, A. K., Kato, E., Kitidis,
892 V., Klein Goldewijk, K., Koven, C., Landschützer, P., Lauvset, S. K., Lefèvre, N., Lenton, A.,
893 Lima, I. D., Metzl, N., Millero, F., Munro, D. R., Murata, A., Nabel, J. E. M. S., Nakaoka, S.,
894 Nojiri, Y., O'Brien, K., Olsen, A., Ono, T., Pérez, F. F., Pfeil, B., Pierrot, D., Poulter, B., Rehder,
895 G., Rödenbeck, C., Saito, S., Schuster, U., Schwinger, J., Séférian, R., Steinhoff, T., Stocker, B.
896 D., Sutton, A. J., Takahashi, T., Tilbrook, B., van der Laan-Luijkx, I. T., van der Werf, G. R., van
897 Heuven, S., Vandemark, D., Viovy, N., Wiltshire, A., Zaehle, S., and Zeng, N.: Global Carbon
898 Budget 2015, Earth Syst. Sci. Data, 7, 349-396, doi:10.5194/essd-7-349-2015, 2015.
899 Locarnini, R.A., Mishonov, A.V., Antonov, J.I., Boyer, T.P., Garcia, H.E., Baranova, O.K., Zweng, M.M.,
900 and Johnson, D.R.: World Ocean Atlas 2009, Volume 1: Temperature, 2010.
901 Ludwig, W., Probst, J. L., and Kempe, S.: predicting the oceanic input of organic carbon by
902 continental erosion, Global Bio geochem. Cy., 10, 23–41, 1996.
903 Maher, D.T., and Eyre, B.D.: Carbon budgets for three autotrophic Australian estuaries: Implications
904 for global estimates of the coastal air-water CO2 flux. Global Biogeochem. Cycles, 26(1),
905 GB1032, 2012.
906 Mayorga, E., Seitzinger, S.P., Harrison, J.A., Dumont, E., Beusen, A.H.W., Bouwman, A.F., Fekete,
907 B.M., Kroeze, C., and Van Drecht, G.: Global Nutrient Export from WaterSheds 2 (NEWS 2):
908 Model development and implementation. Environmental Modelling and Software, 25(7),
909 837-853, 2010.
910 Meybeck, M.: Carbon, nitrogen, and phosphorus transport by world rivers. Am. J. Sci., 282(4), 401-
911 450, 1982.
912 Meybeck, M., Dürr, H. H., and Vörosmarty, C. J.: Global coastal segmentation and its river catchment
913 contributors: A new look at land-ocean linkage, Global Biogeochem. Cy., 20, GB1S90,
914 doi:10.1029/2005GB002540, 2006.
915 Middelburg, J.J., Klaver, G., Nieuwenhuize, J., Wielemaker, A., De Haas, W., Vlug, T., and Van Der
916 Nat, J.F.W.A.: Organic matter mineralization in intertidal sediments along an estuarine
917 gradient. Marine Ecology Progress Series, 132(1-3), 157-168, 1996.
918 NASA/NGA: SRTM Water Body Data Product Specific Guidance, Version 2.0, 2003.
919 Najjar, R.G., Friedrichs, M., and Cai, W.-J. (Editors): Report of The U.S. East Coast Carbon Cycle
920 Synthesis Workshop, January 19-20, 2012. Ocean Carbon and Biogeochemistry Program and
921 North American Carbon Program, 34 pp, 2012.
922 Nihoul, J. C. J., and Ronday, F.: Modèles d'estuaires partiellement stratifiés, Projet Mer, Vol. 10,
923 Service de la Programmation Scientifique, Bruxelles, Belgium, 71–98, 1976.
924 Nixon, S.W., J.W. Ammerman, L.P. Atkinson, V.M. Berounsky, G. Billen, W.C. Boicourt, W.R. Boynton,
925 T.M. Church, D.M. Ditoro, R. Elmgren, J.H. Garber, A.E. Giblin, R.A. Jahnke, N.J. P. Owens,
926 M.E.Q. Pilson, and Seitzinger, S.P.: The fate of nitrogen and phosphorus at the land–sea
927 margin of the North Atlantic Ocean. Biogeochemistry 3, 141–180, 1996.
928 NOAA: National Estuarine Inventory Data Atlas, Volume 1: Physical and Hydrologic Characteristics,
929 National Oceanic and Atmospheric Administration, MD, 1985.
930 Odum, H.T.: Primary Production in Flowing Waters. Limnol. Oceanogr., 1, 102-117, 1956..
931 Paerl, H.W., Valdes, L.M., Peierls, B.L., Adolf, J.E., and Harding Jr, L.W.: Anthropogenic and climatic
932 influences on the eutrophication of large estuarine ecosystems. Limnology and
933 Oceanography, 51(1 II), 448-462, 2006.
934 Preddy, W. S.: The mixing and movement of water in the estuary of the Thames, J. Mar. biol. Ass. UK,
935 33, 645–662, 1954.
936 Press, W. H., Teukolosky, S. A., Vetterling, W. T., and Flannery, B.P.: Numerical Recipes in C: The Art
937 of Scientific Programming, 2nd Edn., Cambridge University Press, USA, 1992.

Biogeosciences Discuss., doi:10.5194/bg-2016-278, 2016
Manuscript under review for journal Biogeosciences
Published: 18 July 2016

938 Pritchard, D. W.: The Equations of Mass Continuity and Salt Continuity in Estuaries, J. Marine Res.,
939 15, 33–42, 1958.
940 Raymond, P.A., Caraco, N.F., and Cole, J.J.: Carbon dioxide concentration and atmospheric flux in the
941 Hudson River. Estuaries, 20(2), 381-390, 1997.
942 Raymond, P.A., Bauer, J.E., and Cole, J.J.: Atmospheric CO2 evasion, dissolved inorganic carbon
943 production, and net heterotrophy in the York River estuary. Limnology and Oceanography,
944 45(8), 1707-1717, 2000.
945 Raymond, P.A., and Hopkinson, C.S.: Ecosystem Modulation of Dissolved Carbon Age in a Temperate
946 Marsh-Dominated Estuary. Ecosystems, 6(7), 694-705, 2003.
947 Raymond, P.A., Hartmann, J., Lauerwald, R., Sobek, S., McDonald, C., Hoover, M., Butman, D., Striegl,
948 R., Mayorga, E., Humborg, C., Kortelainen, P., Dürr, H., Meybeck, M., Ciais, P., and Guth, P.:
949 Global carbon dioxide emissions from inland waters. Nature, 503(7476), 355-359, 2013.
950 Regnier, P., Wollast, R., and Steefel, C.I.: Long-term fluxes of reactive species in macrotidal estuaries:
951 Estimates from a fully transient, multicomponent reaction-transport model. Marine
952 Chemistry, 58(1-2), 127-145, 1997.
953 Regnier, P., Mouchet, A., Wollast, R., and Ronday, F.: A discussion of methods for estimating residual
954 fluxes in strong tidal estuaries, Cont. Shelf Res., 18, 1543–1571, 1998.
955 Regnier, P., and Steefel, C.I.: A high resolution estimate of the inorganic nitrogen flux from the
956 Scheldt estuary to the coastal North Sea during a nitrogen-limited algal bloom, spring 1995.
957 Geochimica et Cosmochimica Acta, 63(9), 1359-1374, 1999.
958 Regnier, P., Vanderborght, J. P., Steefel, C. I., and O'Kane, J. P.: Modeling complex multi-component
959 reactive-transport systems: Towards a simulation environment based on the concept of a
960 Knowledge Base, Appl. Math. Model., 26, 913–927, 2002.
961 Regnier, P., Friedlingstein, P., Ciais, P., Mackenzie, F.T., Gruber, N., Janssens, I.A., Laruelle, G.G.,
962 Lauerwald, R., Luyssaert, S., Andersson, A.J., Arndt, S., Arnosti, C., Borges, A.V., Dale, A.W.,
963 Gallego-Sala, A., Godderis, Y., Goossens, N., Hartmann, J., Heinze, C., Ilyina, T., Joos, F.,
964 LaRowe, D.E., Leifeld, J., Meysman, F.J.R., Munhoven, G., Raymond, P.A., Spahni, R.,
965 Suntharalingam, P., and Thullner, M.: Anthropogenic perturbation of the carbon fluxes from
966 land to ocean. Nature Geosci, 6(8), 597-607, 2013a.
967 Regnier, P., Arndt, S., Goossens, N., Volta, C., Laruelle, G.G., Lauerwald, R., and Hartmann, J.:
968 Modelling Estuarine Biogeochemical Dynamics: From the Local to the Global Scale. Aquatic
969 Geochemistry, 19(5-6), 591-626, 2013b.
970 Riemann, B., Simonsen, P., and Stensgaard, L.: The carbon and chlorophyll content of phytoplankton
971 from various nutrient regimes. Journal of Plankton Research, 11 (5), 1037-1045, 1989.
972 Sarma, V.V.S.S., Viswanadham, R., Rao, G.D., Prasad, V.R., Kumar, B.S.K., Naidu, S.A., Kumar, N.A.,
973 Rao, D.B., Sridevi, T., Krishna, M.S., Reddy, N.P.C., Sadhuram, Y., and Murty, T.V.R.: Carbon
974 dioxide emissions from Indian monsoonal estuaries. Geophysical Research Letters, 39(3),
975 L03602, 2012.
976 Savenije, H.H.G.: A one-dimensional model for salinity intrusion in alluvial estuaries. Journal of
977 Hydrology, 85(1-2), 87-109, 1986.
978 Savenije, H.H.G.: Lagrangian solution of St. Venant's equations for alluvial estuary. Journal of
979 Hydraulic Engineering, 118(8), 1153-1163, 1992.
980 Savenije, H. H. G. (Ed.): Salinity and Tides in Alluvial Estuaries, 1st Edn., Elsevier, Amsterdam, 2005.
981 Savenije, H. H. G. (Ed.): Salinity and Tides in Alluvial Estuaries, 2nd Edn., available at:
982 http://salinityandtides.com (last access: 8 March 2015), 2012.
983 Shih, J.-S., Alexander, R.B., Smith, R.A., Boyer, E.W., Schwarz, G.E., and Chung, S.: An initial SPARROW
984 model of land use and in-stream controls on total organic carbon in streams of the
985 conterminous United States, U. S. Geological Survey, Reston, Virginia, 2010.
986 Signorini, S.R., Mannino, A., Najjar Jr, R.G., Friedrichs, M.A.M., Cai, W.J., Salisbury, J., Wang, Z.A.,
987 Thomas, H., and Shadwick, E.: Surface ocean pCO2 seasonality and sea-air CO2 flux

estimates for the North American east coast. Journal of Geophysical Research C: Oceans, 118(10), 5439-5460, 2013.

Soetaert, K., and Herman, P.M.J.: Nitrogen dynamics in the Westerschelde estuary (SW Netherlands) estimated by means of the ecosystem model MOSES. Hydrobiologia, 311(1-3), 225-246, 1995.

Stets, E.G., and Strieg, R.G.: Carbon export by rivers draining the conterminous united states. Inland Waters, 2(4), 177-184, 2012.

Stigter, C., and Siemons, J.: Calculation of longitudinal salt distribution in estuaries as function of time, Publication Delft Hydraulics Laboratory, 52, The Netherlands, 1967.

Thieu, V., Mayorga, E., Billen, G., and Garnier, J.: Subregional and downscaled global scenarios of nutrient transfer in river basins: Seine-Somme-Scheldt case study. Global Biogeochemical Cycles, 24(2) , 2010.

Tian, H., Chen, G., Liu, M., Zhang, C., Sun, G., Lu, C., Xu, X., Ren, W., Pan, S., and Chappelka, A.: Model estimates of net primary productivity, evapotranspiration, and water use efficiency in the terrestrial ecosystems of the southern United States during 1895-2007. Forest Ecology and Management, 259(7), 1311-1327, 2010.

Tian, H., Chen, G., Zhang, C., Liu, M., Sun, G., Chappelka, A., Ren, W., Xu, X., Lu, C., Pan, S., Chen, H., Hui, D., McNulty, S., Lockaby, G., and Vance, E.: Century-Scale Responses of Ecosystem Carbon Storage and Flux to Multiple Environmental Changes in the Southern United States. Ecosystems, 15(4), 674-694, 2012.

U. S. Fish and Wildlife Service. 2014. National Wetlands Inventory website. U.S. Department of the Interior, Fish and Wildlife Service, Washington, D.C. http://www.fws.gov/wetlands/, last accessed: February 2015.

Vanderborght, J.P., Wollast, R., Loijens, M., and Regnier, P.: Application of a transport-reaction model to the estimation of biogas fluxes in the Scheldt Estuary. Biogeochemistry, 59(1-2), 207-237, 2002.

Vanderborght, J.P., Folmer, I., Aguilera, D.R., Uhrenholdt, T., and Regnier, P.: Reactive-transport modelling of a river-estuarine-coastal zone system: application to the Scheldt estuary. Mar. Chem. 106, 92-110, 2007.

Van der Burgh, P.: Ontwikkeling van een methode voor het voorspellen van zoutverdelingen in estuaria, kanalen and zeeen, Rijkswaterstaat Rapport, The Netherlands, 1972.

Volta, C., Arndt, S., Savenije, H.H.G., Laruelle, G.G., and Regnier, P.: C-GEM (v 1.0): a new, cost-efficient biogeochemical model for estuaries and its application to a funnel-shaped system. Geosci. Model Dev., 6(4), 5645-5709, 2014.

Volta, C., Laruelle, G. G., and Regnier, P.: Regional carbon and CO_2 budgets of North Sea tidal estuaries, Estuarine, Coastal and Shelf Science, 176, 76-90, 2016a.

Volta, C., Laruelle, G. G., Arndt, S., and Regnier, P.: Linking biogeochemistry to hydro-geometrical variability in tidal estuaries: a generic modeling approach, Hydrol. Earth Syst. Sci., 20, 991-1030, doi:10.5194/hess-20-991-2016, 2016b.

Vörösmarty, C.J., Fekete, B., and Tucker, B.A.: River Discharge Database, Version 1.0 (RivDIS v1.0), Volumes 0 through 6. A contribution to IHP-V Theme 1. Technical Documents in Hydrology Series. UNESCO, Paris, 1996.

Wang, Z.A., and Cai, W.J.: Carbon dioxide degassing and inorganic carbon export from a marsh-dominated estuary (the Duplin River): A marsh CO2 pump. Limnology and Oceanography, 49(2), 341-354, 2004.

Biogeosciences Discuss., doi:10.5194/bg-2016-278, 2016
Manuscript under review for journal Biogeosciences
Published: 18 July 2016

1035 **Table 1:** Estimates of total annual riverine input from watersheds to estuaries (Tg C yr^{-1}). The ranges
1036 are based on Stets and Striegl (2012), Global NEWS (Mayorga et al. 2010), Hartmann et al. (2009),
1037 SPARROW (Shih et al. 2010) and DLEM (Tian et al. 2010, 2012). Modified from Najjar et al. 2012.

	DIC	DOC	POC	TOTAL
NAR	0.2-0.8	0.3-2.1	0.1-0.2	0.6-3.1
MAR	1.4-1.8	0.5-2.3	0.1-0.3	2.0-4.4
SAR	0.4-1.4	0.9-1.6	0.1-0.2	1.4-3.2
TOTAL	2.0-4.0	1.7-6.0	0.3-0.7	4.0-10.7

1038
1039
1040

Biogeosciences Discuss., doi:10.5194/bg-2016-278, 2016
Manuscript under review for journal Biogeosciences
Published: 18 July 2016

1041 **Table 2:** State variables and processes explicitly implemented in CGEM.

State variables		
Name	**Symbol**	**Unit**
Suspended Particulate Mater	SPM	gL^{-1}
Total Organic Carbon	TOC	µM C
Nitrate	NO_3	µM N
Ammonium	NH_4	µM N
Phosphate	DIP	µM P
Dissolved Oxygen	DO	µM O_2
Phytoplankton	Phy	µM C
Dissolved Silica	dSi	µM Si
Dissolved Inorganic Carbon	DIC	µM C
Biogeochemical reactions		
Name	**Symbol**	**Unit**
Gross primary production	GPP	µM C s^{-1}
Net primary production	NPP	µM C s^{-1}
Phytoplankton mortality	M	µM C s^{-1}
Aerobic degradation	R	µM C s^{-1}
Denitrification	D	µM C s^{-1}
Nitrification	N	µM N s^{-1}
O_2 exchange with the atmosphere	FO_2	µM O_2 s^{-1}
CO_2 exchange with the atmosphere	FCO_2	µM C s^{-1}
SPM erosion	E_{SPM}	gL^{-1} s^{-1}
SPM deposition	D_{SPM}	gL^{-1} s^{-1}

1042

1043

Biogeosciences Discuss., doi:10.5194/bg-2016-278, 2016
Manuscript under review for journal Biogeosciences
Published: 18 July 2016

1044 **Table 3**: Published local annually averaged estimates of $\overline{FCO_2}$ for estuaries along the East coast of
1045 the US.

Name	Longitude	latitude	$\overline{FCO_2}$	Reference
Altamaha Sound	-81.3	31.3	32.4	Jiang et al. (2008)
Bellamy	-70.9	43.2	3.6	Hunt et al. (2010)
Cocheco	-70.9	43.2	3.1	Hunt et al. (2010)
Doboy Sound	-81.3	31.4	13.9	Jiang et al. (2008)
Great Bay	-70.9	43.1	3.6	Hunt et al. (2011)
Little Bay	-70.9	43.1	2.4	Hunt et al. (2011)
Oyster Bay	-70.9	43.1	4	Hunt et al. (2011)
Parker River estuary	-70.8	42.8	1.1	Raymond and Hopkinson (2003)
Sapelo Sound	-81.3	31.6	13.5	Jiang et al. (2008)
Satilla River	-81.5	31	42.5	Cai and Wang (1998)
York River	-76.4	37.2	6.2	Raymond et al. (2000)
Hudson River	-74	40.6	13.5	Raymond et al. (1997)
Florida Bay	-80.68	24.96	1.4	Dufore (2012)

1046

1047

Biogeosciences Discuss., doi:10.5194/bg-2016-278, 2016
Manuscript under review for journal Biogeosciences
Published: 18 July 2016

Table 4: Yearly averaged surface area (*S*), fresh water discharge (*Q*), residence time (*Rt*), FCO_2 and *NEM* of all simulated estuaries.

long	lat	*S*	*Q*	*Rt*	$\overline{FCO_2}$	$\overline{NEM}$	FCO_2	*NEM*
degrees	*degrees*	km^2	$m^3 s^{-1}$	*days*	*mol C* m^{-2} yr^{-1}	*mol C* m^{-2} yr^{-1}	10^6 *mol C* yr^{-1}	10^6 *mol C* yr^{-1}
NAR								
-67.25	44.75	7	38.5	15	3.7	-37.4	27	-270
-67.25	45.25	12	73.6	15	6.0	-56.7	71	-666
-67.25	45.25	12	73.6	15	13.8	-56.6	162	-666
-67.75	44.75	3	68.5	4	6.7	-63.5	23	-221
-68.25	44.75	14	69.5	19	4.1	-56.2	58	-791
-68.75	44.75	89	309.9	23	27.4	-58.2	2431	-5163
-69.75	44.25	50	626.6	5	32.3	-74.4	1607	-3703
-70.25	43.75	3	25.8	10	2.1	-21.0	7	-71
-70.75	41.75	288	103.6	958	5.0	-4.0	1428	-1146
-70.75	42.25	63	210.7	40	16.2	-32.9	1025	-2081
-70.75	42.75	17	105.8	3	56.3	-69.0	943	-1155
MAR								
-70.75	43.25	31	29.9	11	21.6	-37.4	662	-1146
-71.25	41.75	257	28.2	808	3.9	-2.5	997	-650
-71.75	41.25	21	112.4	4	35.2	-32.6	726	-672
-72.75	40.75	20	25.4	62	30.7	-21.1	623	-430
-72.75	41.25	10	142.5	2	150.8	-36.9	1578	-386
-72.75	41.75	55	476.6	3	55.9	-45.7	3088	-2523
-73.25	40.75	19	26.8	56	31.4	-28.4	608	-550
-74.25	40.75	1192	608.2	126	15.5	-11.8	18432	-14047
-75.25	38.25	399	80.5	172	13.9	-5.0	5558	-2016
-75.25	38.75	354	31.8	357	7.5	-3.0	2659	-1076
-75.25	39.75	1716	499.0	221	10.0	-7.8	17072	-13439
-75.75	39.25	224	18.3	434	7.5	-2.9	1685	-640
-76.25	39.25	3427	717.1	352	8.1	-5.1	27646	-17352
-76.75	37.25	586	272.3	74	15.0	-10.4	8810	-6084
-76.75	37.75	154	36.3	163	10.7	-6.6	1654	-1023
-76.75	39.25	59	71.2	29	48.6	-34.6	2862	-2038
-77.25	38.25	206	30.2	268	6.1	-3.3	1265	-676
-77.25	38.75	568	259.2	118	16.7	-10.8	9488	-6134
SAR								
-78.25	34.25	48	167.4	7	122.5	-62.4	5916	-3015
-79.25	33.25	47	56.3	42	43.4	-36.5	2056	-1728
-79.25	33.75	45	291.4	8	85.1	-78.7	3843	-3551
-79.75	33.25	25	33.8	15	37.9	-32.8	956	-828
-80.25	32.75	25	31.0	50	48.8	-42.5	1214	-1057
-80.25	33.25	92	75.5	61	62.7	-61.2	5769	-5625
-80.75	32.25	71	21.1	182	12.9	-7.0	918	-501
-80.75	32.75	164	63.1	95	20.6	-11.5	3372	-1879
-81.25	31.75	92	71.7	45	25.7	-20.9	2361	-1926
-81.25	32.25	130	379.8	11	51.7	-39.2	6732	-5097
-81.75	30.75	34	18.7	61	17.5	-14.7	602	-505
-81.75	31.25	130	17.7	294	5.5	-4.0	713	-523
-81.75	31.75	56	350.5	4	72.7	-67.4	4068	-3770

Biogeosciences Discuss., doi:10.5194/bg-2016-278, 2016
Manuscript under review for journal Biogeosciences
Published: 18 July 2016

1051 **Table 5:** Seasonal contribution to FCO_2 and *NEM* in each the sub-region. The seasons displaying the
1052 highest percentages are indicated in bold.

Region	*NEM*	winter	spring	summer	fall	FCO_2	winter	spring	summer	fall
	mol C y^{-1}	%	%	%	%	mol C y^{-1}	%	%	%	%
NAR	-16.3 10^9	14.7	21.2	**37.0**	27.2	7.2 10^9	26.3	18.9	26.5	**28.3**
MAR	-72.2 10^9	21.9	25.9	**28.8**	23.4	108.3 10^9	**29.8**	23.3	20.7	26.2
SAR	-30.5 10^9	24.6	20.9	**30.3**	24.2	39.2 10^9	26	23.4	**27**	23.6

1053

1054

Biogeosciences Discuss., doi:10.5194/bg-2016-278, 2016
Manuscript under review for journal Biogeosciences
Published: 18 July 2016

1055 **Table 6:** Regressions and associated coefficient of determination between the depth normalized
1056 residence time (S/Q) and -$\overline{NEM}$ */f(T)*, $\overline{FCO_2}$ */f(T)* and *CFilt*.

Region	$-\overline{NEM}/f(T)$	$\overline{FCO_2}/f(T)$	*CFilt*
NAR	$y = 27.84\ x^{-0.17}$ $r^2 = 0.11$	$y = 6.07\ x^{0.00}$ $r^2 = 0.00$	$y = 15.08 \log_{10}(x) + 4.86$ $r^2 = 0.40$
MAR	$y = 26.03\ x^{-0.63}$ $r^2 = 0.86$	$y = 34.36\ x^{-0.58}$ $r^2 = 0.68$	$y = 40.46 \log_{10}(x) + 9.60$ $r^2 = 0.70$
SAR	$y = 28.36\ x^{-0.71}$ $r^2 = 0.76$	$y = 32.82\ x^{-0.66}$ $r^2 = 0.80$	$y = 23.19 \log_{10}(x) + 43.71$ $r^2 = 0.46$
MAR + SAR	$y = 25.85\ x^{-0.64}$ $r^2 = 0.82$	$y = 31.64\ x^{-0.58}$ $r^2 = 0.70$	$y = 33.30 \log_{10}(x) + 24.88$ $r^2 = 0.57$
NAR + MAR + SAR	$y = 28.98\ x^{-0.66}$ $r^2 = 0.82$	$y = 12.98\ x^{-0.33}$ $r^2 = 0.30$	$y = 40.64 \log_{10}(x) + 11.84$ $r^2 = 0.70$

1057

1058

Biogeosciences Discuss., doi:10.5194/bg-2016-278, 2016
Manuscript under review for journal Biogeosciences
Published: 18 July 2016

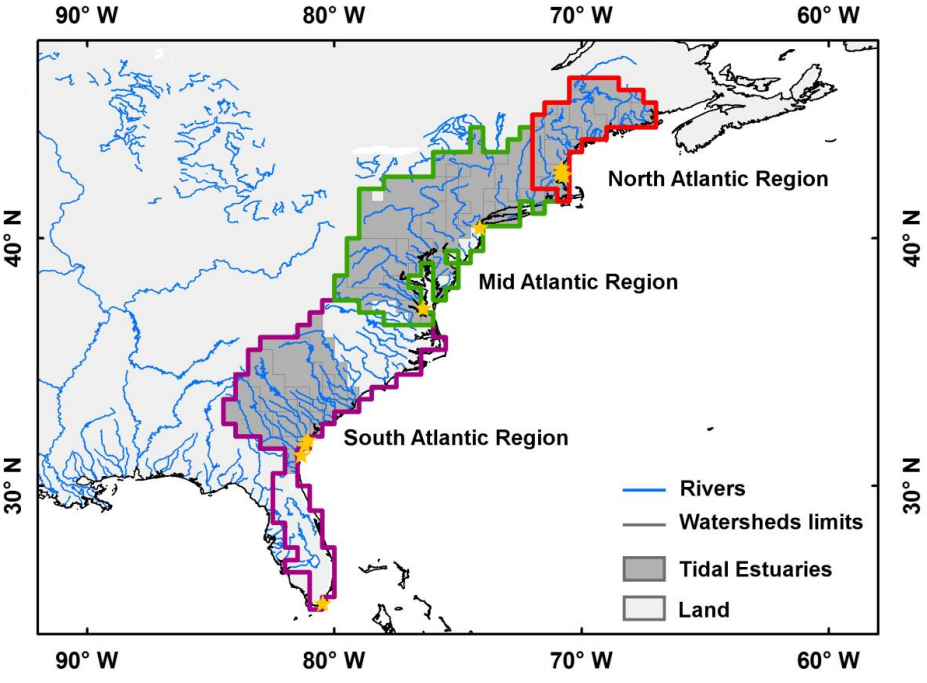

1059

1060 **Figure 1**: Limits of the 0.5 degrees resolution watersheds corresponding to tidal estuaries of the East
1061 coast of the US. 3 sub-regions are delimited with colors and orange stars represent the location of
1062 previous studies.

1063

Biogeosciences Discuss., doi:10.5194/bg-2016-278, 2016
Manuscript under review for journal Biogeosciences
Published: 18 July 2016

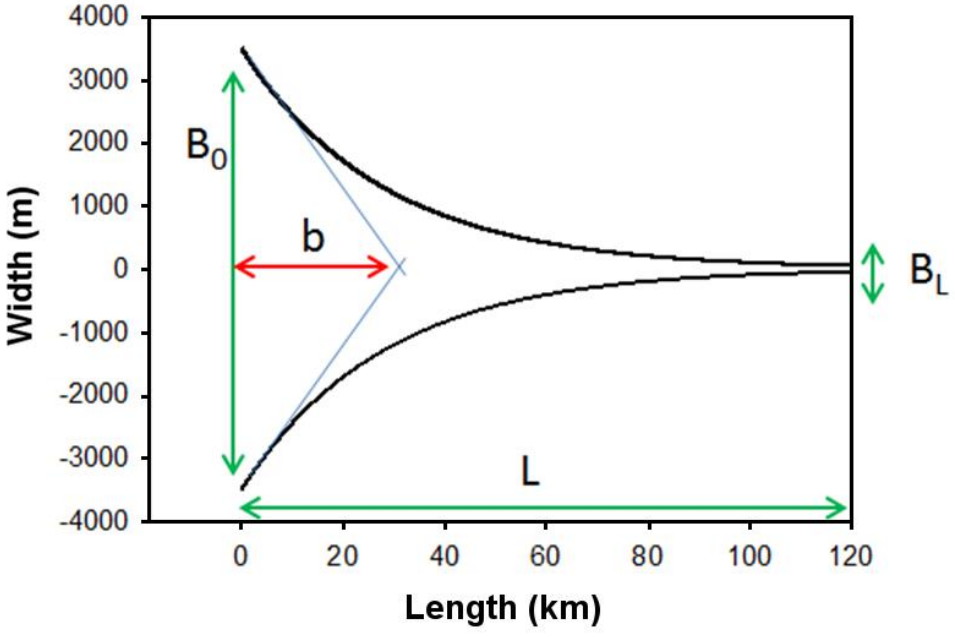

1064

1065 **Figure 2:** Idealized estuarine geometry and main parameters. Parameters indicated by green arrows
1066 are measured, b is calculated. See section 2.3.1 for further details.

1067

Biogeosciences Discuss., doi:10.5194/bg-2016-278, 2016
Manuscript under review for journal Biogeosciences
Published: 18 July 2016

1068

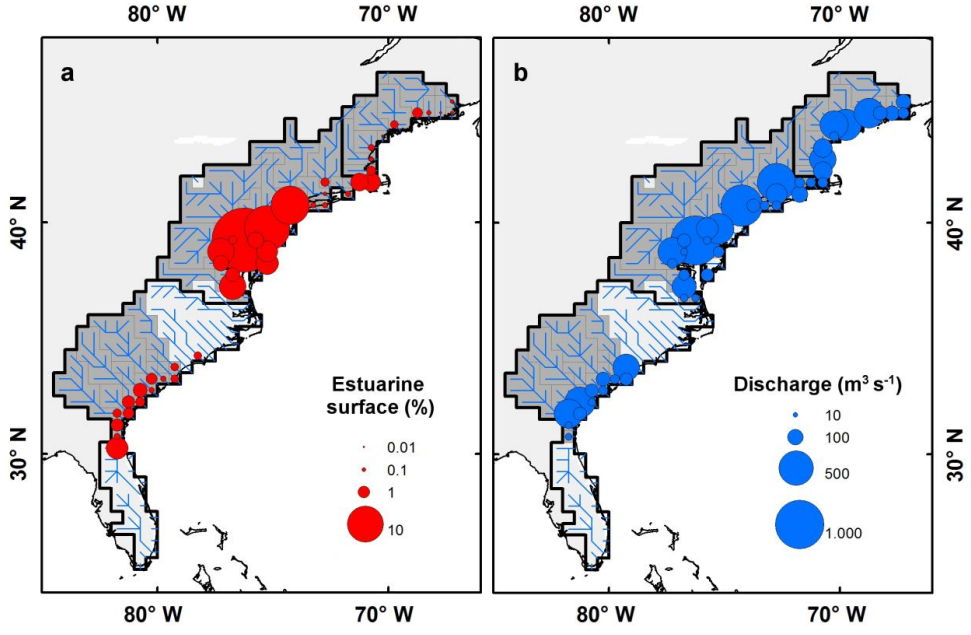

1069

1070 **Figure 3:** Estuarine surface area (a) and mean annual freshwater discharge (b) for each tidal estuary
1071 of the East coast of the US. Estuarine surface area are expressed as percentage of the entire surface
1072 area of the region (19830 km^2)

1073

Biogeosciences Discuss., doi:10.5194/bg-2016-278, 2016
Manuscript under review for journal Biogeosciences
Published: 18 July 2016

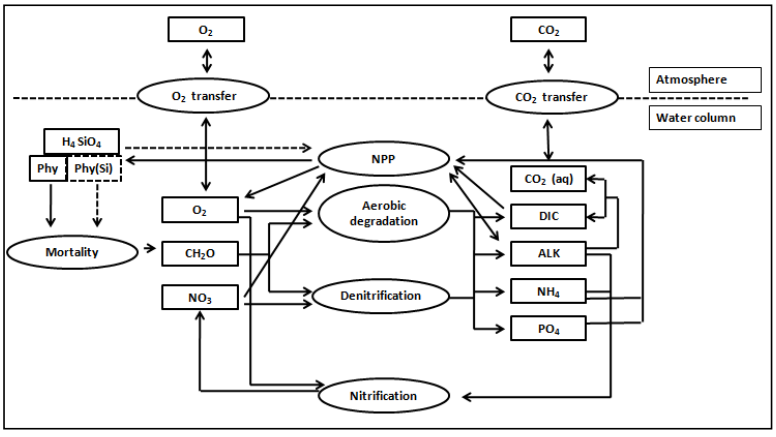

Figure 4: Conceptual scheme of the biogeochemical module of C-GEM used in this study. State-variables and processes are represented by boxes and oval shapes, respectively. Modified from Volta et al., 2014.

Biogeosciences Discuss., doi:10.5194/bg-2016-278, 2016
Manuscript under review for journal Biogeosciences
Published: 18 July 2016

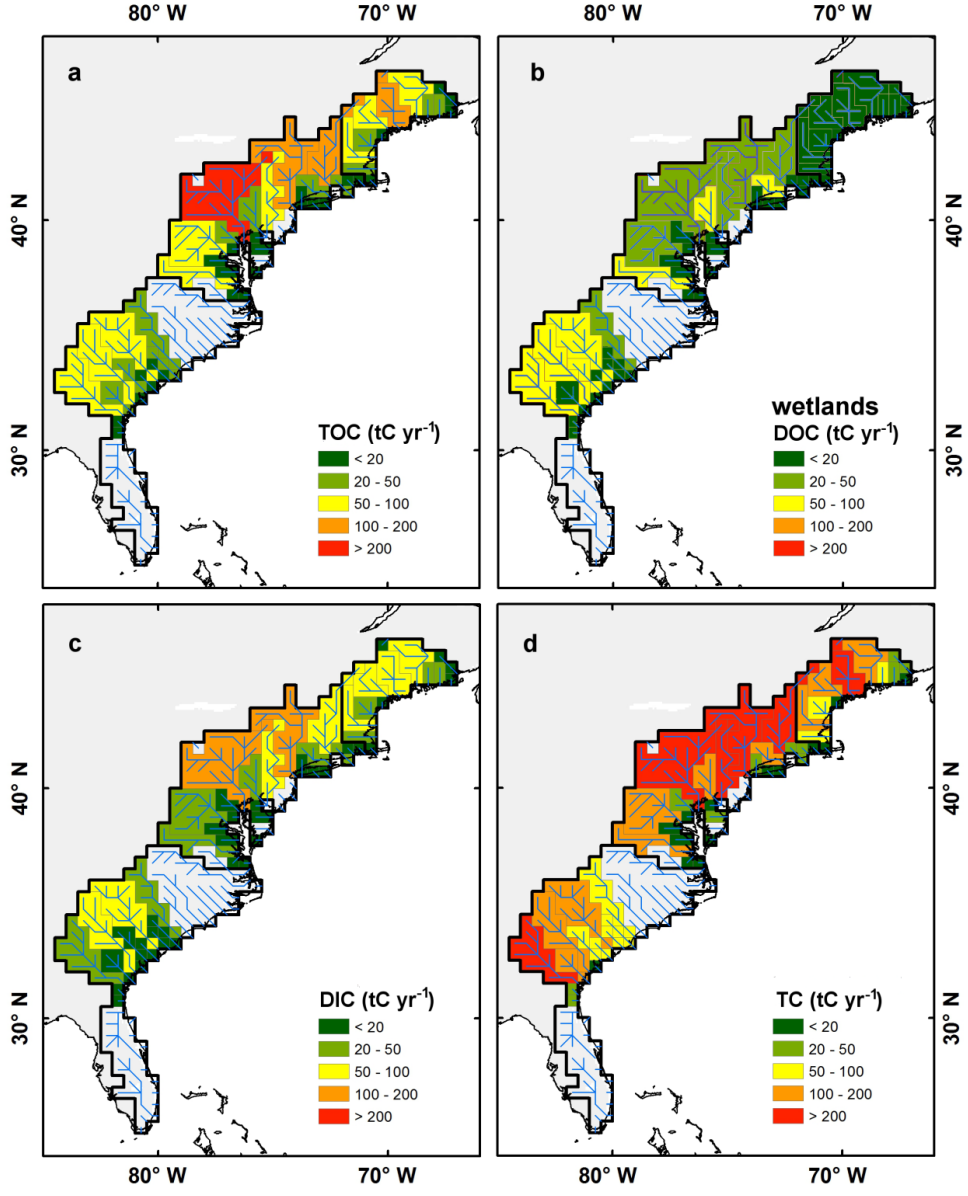

1079

1080 **Figure 5:** Annual river carbon loads of TOC (a), annual DOC fluxes from wetlands (b), annual river
1081 carbon loads of DIC (c) and annual TC fluxes (d). All fluxes are indicated per watershed.

1082

Biogeosciences Discuss., doi:10.5194/bg-2016-278, 2016
Manuscript under review for journal Biogeosciences
Published: 18 July 2016

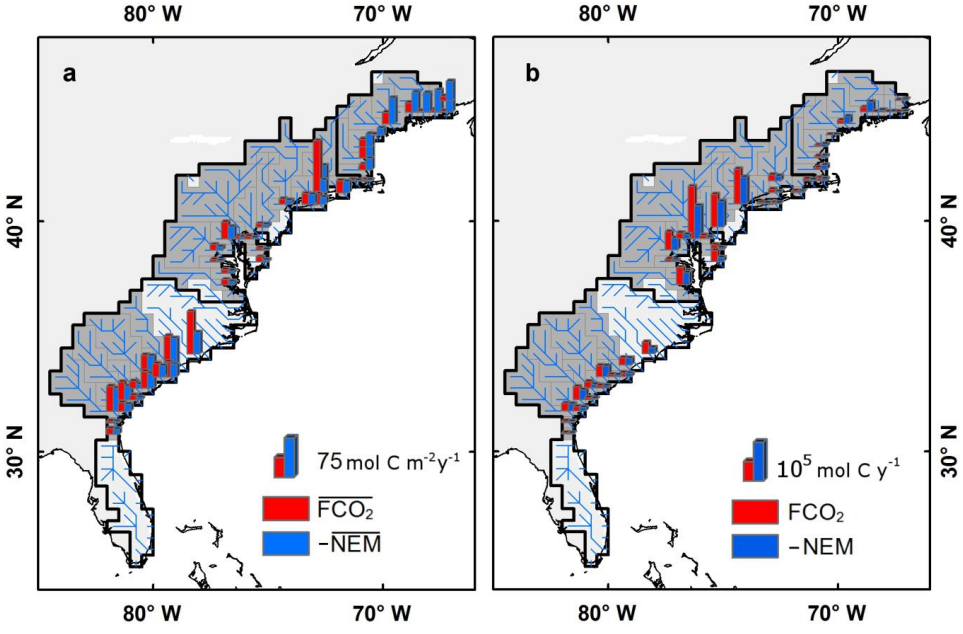

1083

1084 **Figure 6:** Spatial distribution of spatially averaged value (a) and integrated value (b) of mean annual
1085 FCO_2 (red) and -*NEM* (blue) along the East coast of the US. On panel a, the notation with overbars
1086 ($\overline{FCO_2}$ and -$\overline{NEM}$) represents rates per unit surface. For the sake of the comparison with $\overline{FCO_2}$,
1087 figure 6 displays -$\overline{NEM}$ because the model predicts that all estuaries in this region are net
1088 heterotrophic.

1089

Biogeosciences Discuss., doi:10.5194/bg-2016-278, 2016
Manuscript under review for journal Biogeosciences
Published: 18 July 2016

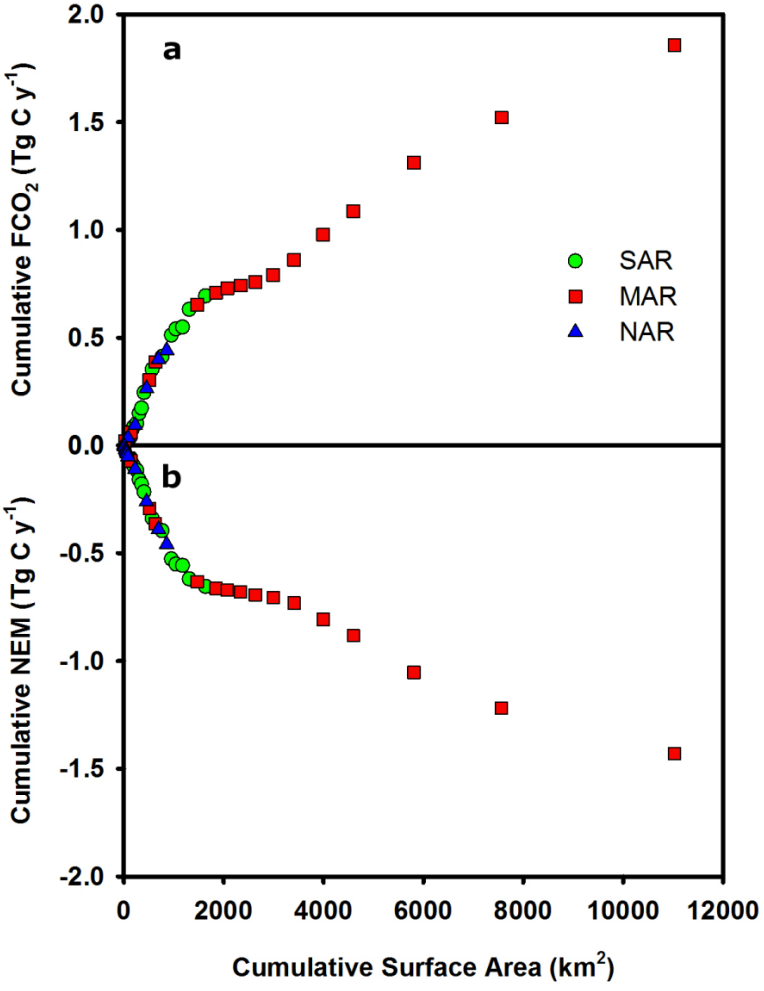

1090

1091 **Figure 7:** The Cumulative *FCO_2* (a) and *NEM* (b) as functions of the cumulative estuarine surface area.
1092 Systems are sorted by increasing surface area.

1093

Biogeosciences Discuss., doi:10.5194/bg-2016-278, 2016
Manuscript under review for journal Biogeosciences
Published: 18 July 2016

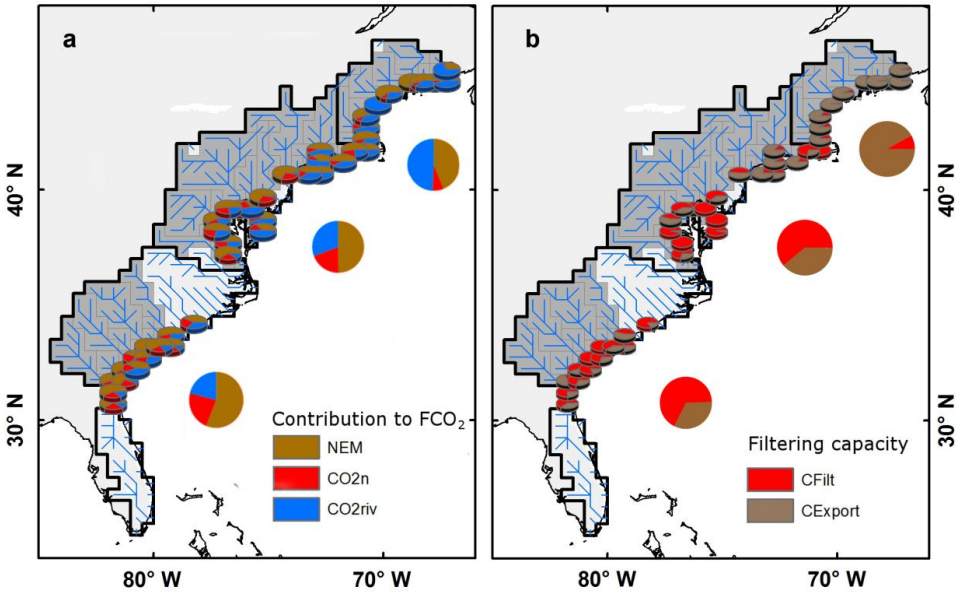

1094

1095 **Figure 8:** Contribution of *NEM*, nitrification and riverine waters super-saturated waters to the mean
1096 annual FCO_2 (a). Spatial distribution of mean annual carbon filtration capacities (*CFilt*) and export
1097 (*CExport*) along the East coast of the US (b).

1098

Biogeosciences Discuss., doi:10.5194/bg-2016-278, 2016
Manuscript under review for journal Biogeosciences
Published: 18 July 2016

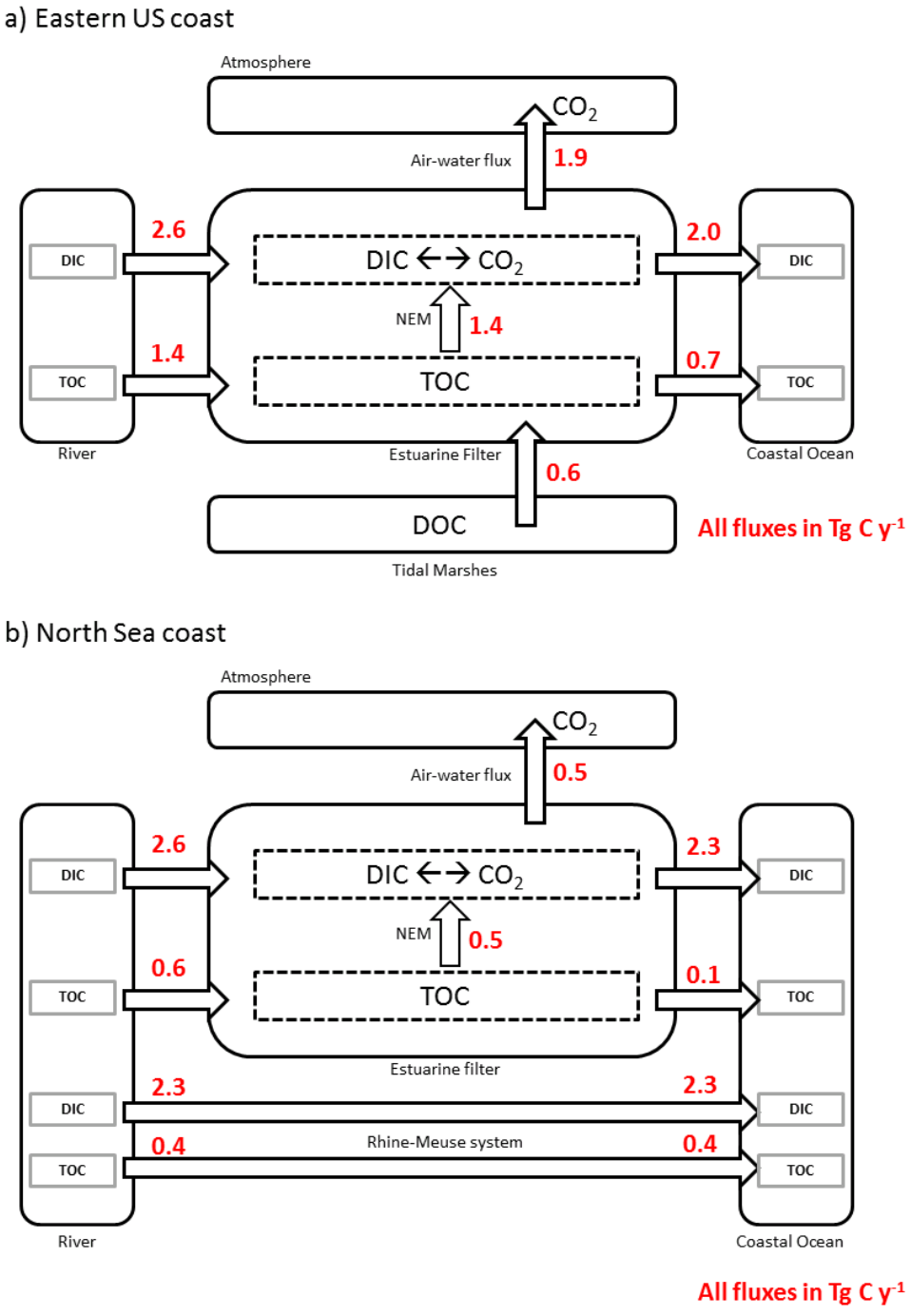

1099

1100 **Figure 9:** Annual carbon budget of the estuaries of the East coast of the US (a) and of the coast of
1101 the North Sea (b, modified from Volta et al., 2016a).

Biogeosciences Discuss., doi:10.5194/bg-2016-278, 2016
Manuscript under review for journal Biogeosciences
Published: 18 July 2016

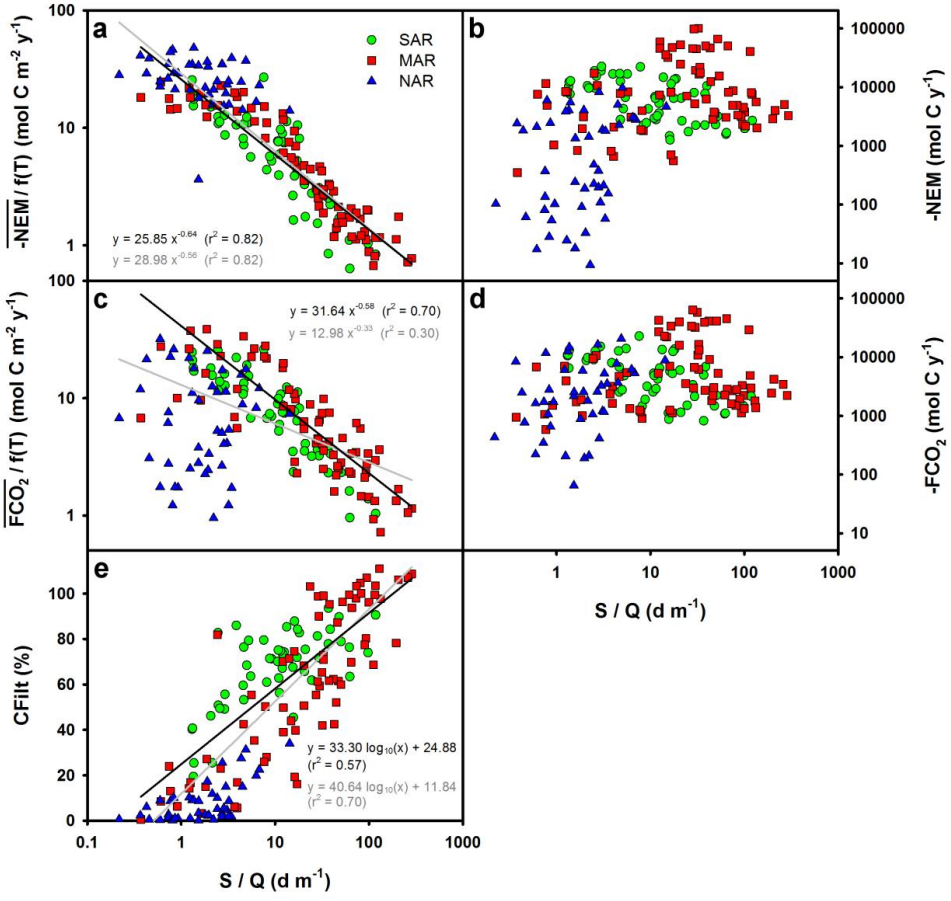

1102

1103 **Figure 10:** -$\overline{NEM}$ / *f(T)* (a), -NEM (b), $\overline{FCO_2}$ / *f(T)* (c), *FCO_2* (d) and *CFilt* (e) as functions of the depth

1104 normalized residence time expressed as the ratio of the estuarine surface S and the river discharge

1105 Q. The grey and black lines are the best fitted regressions obtained using all the point or only the

1106 estuaries from the MAR and SAR regions, respectively.

1107